

## Article

# Real-Time Precise Orbit Determination of Low Earth Orbit Satellites Based on GPS and BDS-3 PPP B2b Service

Yali Shi <sup>1</sup>, Tianhe Xu <sup>1</sup>, Min Li <sup>1,\*</sup>, Kai Wei <sup>2</sup>, Shuai Wang <sup>3</sup> and Dixin Wang <sup>1</sup>

<sup>1</sup> Institute of Space Sciences, Shandong University, Weihai 264209, China; 202121029@mail.sdu.edu.cn (Y.S.); thxu@sdu.edu.cn (T.X.); 202221163@mail.sdu.edu.cn (D.W.)

<sup>2</sup> Qilu Aerospace Information Research Institute, Chinese Academy of Sciences, Jinan 250100, China; weikai@aircas.ac.cn

<sup>3</sup> School of Systems Science and Engineering, Sun Yat-Sen University, Guangzhou 510275, China; wangsh523@mail2.sysu.edu.cn

\* Correspondence: limin0614@sdu.edu.cn; Tel.: +86-19563039268

**Abstract:** This study investigates and verifies the feasibility of the precise point positioning (PPP)-B2b enhanced real-time (RT) precise orbit determination (POD) of low Earth orbit (LEO) satellites. The principles and characteristics of matching various PPP-B2b corrections are introduced and analyzed. The performance and accuracy of broadcast ephemeris and PPP-B2b signals are compared and evaluated by referring to the precise ephemeris. The root mean square (RMS) errors in the Global Positioning System (GPS) and BeiDou Navigation Satellite System (BDS)-3 broadcast ephemeris orbits in the along direction are larger than those in the other two (radial and cross) directions, and correspondingly, the along component PPP-B2b corrections are greatest. The continuity and smoothness of the GPS and BDS-3 broadcast ephemeris orbits and clock offsets are improved with the PPP-B2b corrections. The availability of PPP-B2b corrections is comprehensively analyzed for the TJU-01 satellite. Several comparative schemes are adopted for the RT POD of the TJU-01 satellite using the broadcast ephemeris and PPP-B2b corrections. The RT POD performance is improved considerably with the broadcast ephemeris corrected by the PPP-B2b signals. The RMS of the RT orbital errors in the radial, along, and cross directions is 0.10, 0.13, and 0.09 m, respectively, using BDS-3 and GPS PPP-B2b corrections, with reference to the solutions calculated with the precise ephemeris. The accuracy is improved by 5.1%, 43.9%, and 28.7% in the three directions, respectively, relative to that achieved with the broadcast ephemeris. It is concluded that a greater proportion of received PPP-B2b satellite signals corresponds to a greater improvement in the accuracy of the RT POD of the LEO satellite.

**Keywords:** GPS; BDS-3; broadcast ephemeris; real time; PPP-B2b; precise orbit determination



**Citation:** Shi, Y.; Xu, T.; Li, M.; Wei, K.; Wang, S.; Wang, D. Real-Time Precise Orbit Determination of Low Earth Orbit Satellites Based on GPS and BDS-3 PPP B2b Service. *Remote Sens.* **2024**, *16*, 833. <https://doi.org/10.3390/rs16050833>

Academic Editors: Jianguo Yan and Xiaogong Hu

Received: 15 December 2023

Revised: 14 February 2024

Accepted: 26 February 2024

Published: 28 February 2024



**Copyright:** © 2024 by the authors. Licensee MDPI, Basel, Switzerland. This article is an open access article distributed under the terms and conditions of the Creative Commons Attribution (CC BY) license (<https://creativecommons.org/licenses/by/4.0/>).

## 1. Introduction

For the last few years, with an increasing frequency of space missions, there has been a growing need for the precise and real-time (RT) orbit determination of low Earth orbit (LEO) satellites, which has been widely studied [1–3]. According to the actual Global Positioning System (GPS) broadcast ephemeris with the Jet Propulsion Laboratory's global differential GPS corrections, the root mean square (RMS) error in the three-dimensional (3D) direction of the RT POD of the Challenging Mini Satellite Payload (CHAMP) spacecraft is 30 cm [4]. The RT POD of Meteorological Operational Satellite-A (MetOp-A) has been performed using observations recorded by the global navigation satellite system (GNSS) receiver of an onboard atmospheric sounding instrument and the results indicate that the accuracy can reach 0.5 m in the three axial directions of the GPS broadcast ephemeris [5]. Through dynamic model compensation, the standard deviation (STD) of the RT POD of the Fengyun-3C using BDS/GPS pseudo-range measurements can reach the meter level [6].

The global networking of the Beidou Global Navigation Satellite System (BDS) was completed in 2020. PPP-B2b is one of the services provided by the BDS-3 navigation system and is used to enhance precise point positioning (PPP). The PPP-B2b signal is used as the broadcast channel, and BDS-3 geosynchronous orbit (GEO) satellites broadcast correction information to users. This signal provides users with RT PPP services [7]. The widespread application of PPP-B2b has coincided with the study of PPP-B2b by many scholars [7–13]. Yang et al. reported the physical properties of PPP-B2b including the area covered by its signal and its accuracy for PPP [14]. Liu et al. found the precision of PPP enhanced by PPP-B2b products is higher than that of RT products from Wuhan University [8]. Tao et al. compared the kinematics PPP accuracy when using BDS-3 PPP-B2b with that when using the GPS and an RT service (RTS) provided by the National Centre for Space Studies [11]. Chen et al. evaluated the performance of RT products provided by the BDS [15].

Many scholars have studied RT corrections for the RT POD of LEO satellites. When using the high-quality RT GPS precise ephemeris and clocks from the German Space Operations Center for the RT POD of the Terra Synthetic Aperture Radar-X mission, the RMS error of orbits was 2.1 cm [16]. Xiao et al. (2022) explored an innovative way of controlling the receiver clock offset quality in the RT POD for the Gravity Recovery and Climate Experiment (GRACE) follow-on mission and demonstrated that the RMS error in the three orthogonal directions of the RT POD of the mission using the German Research Centre for Geosciences BeiDou multi-GNSS product is about 8 cm and that using the National Centre for Space Studies RT ephemeris is approximately 10 cm [17]. Using high-precision RT orbit and clock offset products from IGS-RTS, the accuracy of the RT POD of GRACE-C in the radial direction using spaceborne GPS observations reaches the centimeter level [18]. In summary, the accuracy of the RT POD of LEO satellites is improved by RT corrections.

A highly accurate broadcast ephemeris is needed for the RT POD of an LEO satellite. The accuracy of a broadcast ephemeris can be improved using the PPP-B2b service. Although spaceborne GNSS data receivers do not receive PPP-B2b corrections currently, chips that can receive the broadcast ephemeris and PPP-B2b signal at the same time have been manufactured, e.g., the K803 board manufactured by SinoGNSS. Therefore, the RT POD of LEO satellites can be performed with the broadcast ephemeris and PPP-B2b services based on GPS and BDS observations. The present study takes the Tianjin University Satellite No. 1 (TJU-01) as an example to verify the feasibility of the RT POD of LEO satellites with the broadcast ephemeris and PPP-B2b service. It is the first to analyze the GPS and BDS LEO satellite orbit determination based on the PPP-B2b service. The TJU-01 satellite is an essential component of the Yunyao constellation, with more than 20 satellites to be networked. TJU-01 was launched in December 2021, has a mass of 20.53 kg, and operates in a 512 km Sun-synchronous orbit. It is equipped with an onboard GPS and BDS-2/3 multi-GNSS receiver for GNSS occultation and POD service. The RT POD performance of TJU-01 with a PPP-B2b service is demonstrated in detail.

The rest of this article is arranged as follows. The mathematical principles and processing of the RT POD using PPP-B2b with its matching and correction algorithm are introduced and described. The variation characteristics, accuracy, and availability statistics of the PPP-B2b correction are then analyzed. The experimental results of the RT POD of the TJU-01 satellite using PPP-B2b and its improvement are next analyzed. Finally, conclusions are drawn from the results of the research.

## 2. Principle of the Broadcast Ephemeris Correction with the PPP-B2b Service

PPP-B2b has seven types of messages for correcting the broadcast ephemeris and pseudo-range observations. The application of these corrections usually comprises two parts. The first part is the matching of various corrections and the second is the correction of the broadcast ephemeris and code measurements.

## 2.1. Matching Algorithms of PPP-B2b Messages

There are seven message types in PPP-B2b. These seven message types refer to five types of data, namely the satellite mask, differential code bias (DCB), orbit corrections, clock corrections, and the user ranging accuracy index, as given in Table 1. These PPP-B2b corrections should be matched before being made. The algorithms for PPP-B2b matching and correcting LANV and CNAV ephemerides during the real-time precise orbit determination (RT POD) of LEO satellites are identical to those used in other scenarios, such as traditional PPP, with no distinction. Firstly, the Issue of Data State Space Representation (IOD SSR) should match between various types of messages before the corrections can be used together [10]. Secondly, the Issue of Data of the PRN mask (IODP) included in message types 4, 5, and 6 must be the same as the IODP of message type 1 before the corrections are made. The PPP-B2b Issue of Data, Navigation (IODN) should be consistent with the GNSS IOD. An inconsistency indicates that the GNSS has updated its broadcast ephemeris. The previous broadcast ephemeris should be used for matching the PPP-B2b until the PPP-B2b IODN is updated and matches the GNSS IOD. Again, for the same satellite, the version number of the clock correction message (IOD of the correction, IOD Corr) should be the same as in the orbit correction, such that the clock correction and orbit correction (in message type 2) match each other. Finally, the broadcast time of the broadcast ephemeris must match the broadcast time of its corresponding correction message and must not exceed the validity period of the correction. Thus, the correction message can be used [19]. The validity periods of various message types of PPP-B2b are given in Table 1.

**Table 1.** Validity periods of various corrections.

The Content of Correction	Message Type	Nominal Validity	Update Interval
Satellite mask	1	86,400 s	48 s
Orbit correction	2, 6, 7	96 s	48 s
Clock correction	3	86,400 s	12 s
Differential code bias	4, 6, 7	12 s	6 s
User ranging accuracy index	2, 5, 6, 7	96 s	48 s

## 2.2. Correction Algorithm

After the PPP-B2b corrections are matched, we obtain the corrected satellite position with the orbit correction message:

$$X_{\text{orbit}} = X_{\text{broadcast}} - \delta X \quad (1)$$

where  $X_{\text{broadcast}}$  denotes the 3D coordinates of satellite positions calculated through the broadcast ephemeris.  $\delta X = [e_{\text{radial}} \ e_{\text{cross}} \ e_{\text{along}}] \cdot \delta O$  is the orbit correction message, where  $e_{\text{radial}} = \frac{r}{|r|}$ ,  $e_{\text{cross}} = \frac{r \times \dot{r}}{|r \times \dot{r}|}$ , and  $e_{\text{along}} = e_{\text{cross}} \times e_{\text{radial}}$ , with  $r$  being the 3D position coordinate vector and  $\dot{r}$  being the 3D velocity coordinate vector in the ECEF coordinate system. These vectors are obtained from the broadcast ephemeris.  $e_i$  denotes a unit vector with the subscript  $i = \{\text{radial}, \text{along}, \text{cross}\}$  indicating the direction in the centroid orbit coordinate system.  $\delta O$  is the 3D orbit correction vector broadcast by the PPP-B2b service. The equation for obtaining the clock offset of PPP-B2b is

$$t_{\text{satellite}} = t_{\text{broadcast}} - \frac{c_0}{c} \quad (2)$$

where  $t_{\text{satellite}}$  is the clock offset of PPP-B2b,  $t_{\text{broadcast}}$  is the uncorrected clock offset calculated from the broadcast ephemeris,  $c$  is a constant representing the speed of light, and  $c_0$  is the clock offset correction. The equation of the DCB correction algorithm is

$$\tilde{l} = l_{\text{broadcast}} - DCB_{B2b} \quad (3)$$

where  $l_{broadcast}$  denotes the code measurements corresponding to the ranging signals,  $\tilde{l}$  denotes the corrected code measurements corresponding to the ranging signals, and  $DCB_{B2b}$  denotes the DCB correction message of the corresponding ranging signal. The dual-frequency ionosphere-free combination code measurements obtained after the DCB correction are

$$\tilde{l} = \frac{\gamma \tilde{l}_1 - \tilde{l}_2}{\gamma - 1} = \frac{\gamma l_1 - l_2}{\gamma - 1} - \frac{\gamma DCB_1 - DCB_2}{\gamma - 1} \quad (4)$$

$$\gamma = \frac{f_1^2}{f_2^2} \quad (5)$$

where  $f_1$  is the center frequency of carrier phase  $l_1$  and  $f_2$  is the center frequency of the carrier phase and  $DCB_1$  and  $DCB_2$  are the corresponding DCB correction messages. The DCB correction is used to correct pseudo-range observations. It is also used to correct the clock offset when evaluating the PPP-B2b clock offset in this study.

### 3. Mathematical Models for the RT POD of LEO Satellites

#### 3.1. Preprocessing of Pseudo-Range and Carrier-Phase Measurements after B2b Correction

Compared with ground receivers, LEO satellites travel more quickly and have shorter signal tracking times for GNSS satellites, and their observations thus have greater gross errors. It is thus necessary to preprocess the spaceborne measurements of the LEO satellites. The on-the-fly data-editing method is adopted in preprocessing the RT POD data of LEO satellites using PPP-B2b [2]. PPP-B2b corrections are used for correcting the broadcast ephemeris and pseudo-range. Next, in the filtering process, the LEO orbit calculated through dynamic integration combined with each GNSS satellite orbit obtained from the GNSS broadcast ephemeris corrected by PPP-B2b is used to compute each spaceborne GNSS receiver clock offset and then check whether all the satellite pseudo-range residuals exceed a given tolerance [20]. If so, the pseudo-range observations with gross errors are eliminated. The carrier-phase measurements are processed using the same method. If necessary, the above process is repeated to delete faulty error measurements and thus ensure that the data are correct.

#### 3.2. Observation Model

The observation model considering the LEO dynamic parameters is presented in the following. An LEO satellite flies above the troposphere, and the tropospheric delay is thus ignored. The linearization ionosphere-free observation model for the RT POD of LEO satellites without tropospheric delay is expressed as [21]

$$P_{leo,IF,i}^G = -u_{leo}^G \Phi(t_s, t_0)^{leo} o^{leo} + c\delta t_{leo,i}^G + \varepsilon p_{leo,IF,i}^G \quad (6)$$

$$L_{leo,IF,i}^G = -u_{leo}^G \Phi(t_s, t_0)^{leo} o^{leo} + c\delta t_{leo}^G + \lambda_{IF}^G B_{leo,IF}^G + \varepsilon L_{leo,IF,i}^G \quad (7)$$

$$P_{leo,IF,i}^C = -u_{leo}^C \Phi(t_s, t_0)^{leo} o^{leo} + c\delta t_{leo}^C + ISB^{G/C} + \varepsilon p_{leo,IF,i}^C \quad (8)$$

$$L_{leo,IF,i}^C = -u_{leo}^C \Phi(t_s, t_0)^{leo} o^{leo} + c\delta t_{leo}^C + ISB^{G/C} + \lambda_{IF}^C B_{leo,IF}^C + \varepsilon L_{leo,IF,i}^C \quad (9)$$

$$o_0^{leo} = [x_0^{leo}, y_0^{leo}, z_0^{leo}, \dot{x}_0^{leo}, \dot{y}_0^{leo}, \dot{z}_0^{leo}, p_1^{leo}, p_2^{leo}, \dots, p_n^{leo}]^T \quad (10)$$

A superscript G indicates the GPS whereas a superscript C indicates the BDS. A subscript IF indicates ionosphere-free combination observations and a subscript leo indicates an LEO satellite.  $P$  indicates the observed-minus-computed code measurements at the corresponding epoch. Similarly,  $L$  indicates the observed-minus-computed carrier measurements at the corresponding epoch.  $u$  is the unit vector in the direction from the satellite-borne receiver to the navigation satellite.  $\Phi(t_s, t_0)^{leo}$  is the matrix for the transition between epoch  $t_0$  and epoch  $t_s$ .  $o_0^{leo}$  indicates the unknown initial receiver state.

$[x_0^{leo}, y_0^{leo}, z_0^{leo}]^T$  is the 3D position vector of the LEO satellite.  $[\dot{x}_0^{leo}, \dot{y}_0^{leo}, \dot{z}_0^{leo}]^T$  is the 3D velocity vector of the LEO satellite.  $[p_1^{leo}, p_2^{leo}, \dots, p_n^{leo}]^T$  are dynamic parameters including the coefficient of solar pressure  $C_R$ , atmospheric drag coefficient  $C_D$ , and empirical acceleration vectors  $a = [a_R, a_a, a_c]$  in the three axial directions of the centroid orbit coordinate system.  $c$  is a constant representing the speed of light.  $\delta t$  is the spaceborne receiver clock offset.  $ISB^{G/C}$  is the inter-system bias (ISB) parameter between the GPS receiver clock offset and BDS receiver clock offset.  $B$  represents the floating-point solution of ambiguity.  $\lambda$  is the wavelength,  $\epsilon P$  is the code measurements noise, and  $\epsilon L$  is the phase measurements noise. This model is applicable to not only the broadcast ephemeris but also PPP-B2b.

### 3.3. Kalman Filtering Model

In RT POD, Kalman filtering is adopted to calculate all the parameters to be solved considering the model dynamics. The calculated parameters are

$$X = [(o_0^{leo})^T, \delta t_{leo,i}^G, ISB^{G/C}, (B_{leo,IF}^s)^T]^T \quad (11)$$

The Kalman filter is first initialized. The initial state estimate  $\hat{X}_0$  is set as  $X_0^{ref}$  calculated from the kinematic solution based on code observations. The initial state covariance  $\hat{P}_0$  is set as  $\hat{P}_0^{ref}$  in Table 4 [20]. The fourth-order Runge–Kutta scheme with Richardson extrapolation is adopted to calculate the position  $[x_0^{leo}, y_0^{leo}, z_0^{leo}]^T$  and velocity  $[\dot{x}_0^{leo}, \dot{y}_0^{leo}, \dot{z}_0^{leo}]^T$  in the predicted state. The empirical acceleration prediction is

$$\bar{a}_i = e^{-|t_i - t_{i-1}|/\tau} \cdot \hat{a}_{i-1} \quad (12)$$

where  $\tau$  is the time corresponding to the empirical accelerations.  $\hat{a}_{i-1}$  is the prediction of the empirical acceleration at epoch time  $t_{i-1}$  and  $\bar{a}_i$  is the empirical acceleration at epoch time  $t_i$ . In a continuous observation arc, the prediction of the coefficients  $C_R$  and  $C_D$ , the prediction of the spaceborne GPS receiver clock offset  $\delta t$ , and the prediction of the inter-system biases  $ISB^{G/C}$  and the ambiguity parameter  $(B_{leo,IF}^s)^T$  are all constants during the filter propagation process. It is thus concluded that

$$(\bar{C}_R, \bar{C}_D, \delta t_{leo,i}^G, ISB^{G/C}, (B_{leo,IF}^s)^T)_i = (\bar{C}_R, \bar{C}_D, \delta t_{leo,i}^G, ISB^{G/C}, (B_{leo,IF}^s)^T)_{i-1} \quad (13)$$

Firstly, the transition matrix  $\Phi_{i,i-1} = \partial X_i^{ref} / \partial X_{i-1}^{ref}$  is calculated. The predicted state  $\bar{X}$  is then computed as

$$\bar{X}_i = X_i^{ref} + \Phi_{i,i-1}(\hat{X}_{i-1} - X_{i-1}^{ref}) \quad (14)$$

where  $\hat{X}_{i-1}$  denotes the state estimate at the previous epoch  $i - 1$  and  $X_i^{ref}$  is the reference state matrix obtained from the observation information at epoch  $i$ . The covariance matrix  $\bar{P}_i$  is then computed as

$$\bar{P}_i = \Phi_{i,i-1}\hat{P}_{i-1}\Phi_{i,i-1}^T + Q_i \quad (15)$$

During the filtering process, the covariance and bias matrices of satellites that are no longer tracked by the LEO satellites are cleared and those of satellites that are retraced are initialized [2].  $Q_i$  is the increase in covariance resulting from the cumulative effect of the processing noise and  $\hat{P}_{i-1}$  is the covariance of the estimates at epoch  $i - 1$ . The gain matrix  $\bar{K}_i$ , state estimates  $\hat{X}_i$ , and covariance matrix  $\bar{P}_i$  are then obtained according to

$$\bar{K}_i = \bar{P}_i H_i^T (H_i \bar{P} H_i^T + R_i)^{-1} \quad (16)$$

$$\hat{X}_i = \bar{X} + \bar{K}_i L_i \quad (17)$$

$$\hat{P}_i = (I - \bar{K}_i H_i) \bar{P} (I - \bar{K}_i H_i)^T + K_i R_i K_i^T \quad (18)$$

where  $R_i$  is the measurement noise covariance matrix. The non-negativity of the covariance matrix is guaranteed by Equation (18). The design matrix is  $H$ .  $L_i$  denotes the observed-minus-calculated code and phase measurements.

To solve the divergence problem caused by traditional linear Kalman filtering, extended Kalman filtering is adopted for the RT POD of the LEO satellite in this study. Here, the reference state vector  $X_i^{ref}$  is computed through the orbital integration of satellite dynamics as

$$\tilde{X} = X_i^{ref} + x_i \quad (19)$$

where  $x_i = (H_i^T P_i H_i)^{-1} H_i^T P_i L_i$  and  $P_i = R_i^{-1}$  is the weight of the observations. In this study, through high-precision pseudo-range observations, navigation satellite orbits, and clock offsets obtained from the broadcast ephemeris corrected by PPP-B2b, the high-precision 3D coordinate increment of LEO satellites is obtained, and the high-precision orbits are transferred to the next epoch.

### 3.4. Processing Strategy

Dynamic models for the RT POD of the TJU-01 satellite are first introduced. The detailed RT POD strategy is then presented in Tables 2 and 3. This is followed by the setting of parameters relating to the processing noise, as given in Table 4. These parameters are set considering the results of multiple previous experiments.

The GNSS data processing strategy for the TJU-01 satellite RT POD is presented in Table 3.

On the basis of the strategy mentioned above, the data processing is outlined in Figure 1.

**Table 2.** Dynamic model for the RT POD of the TJU-01 satellite.

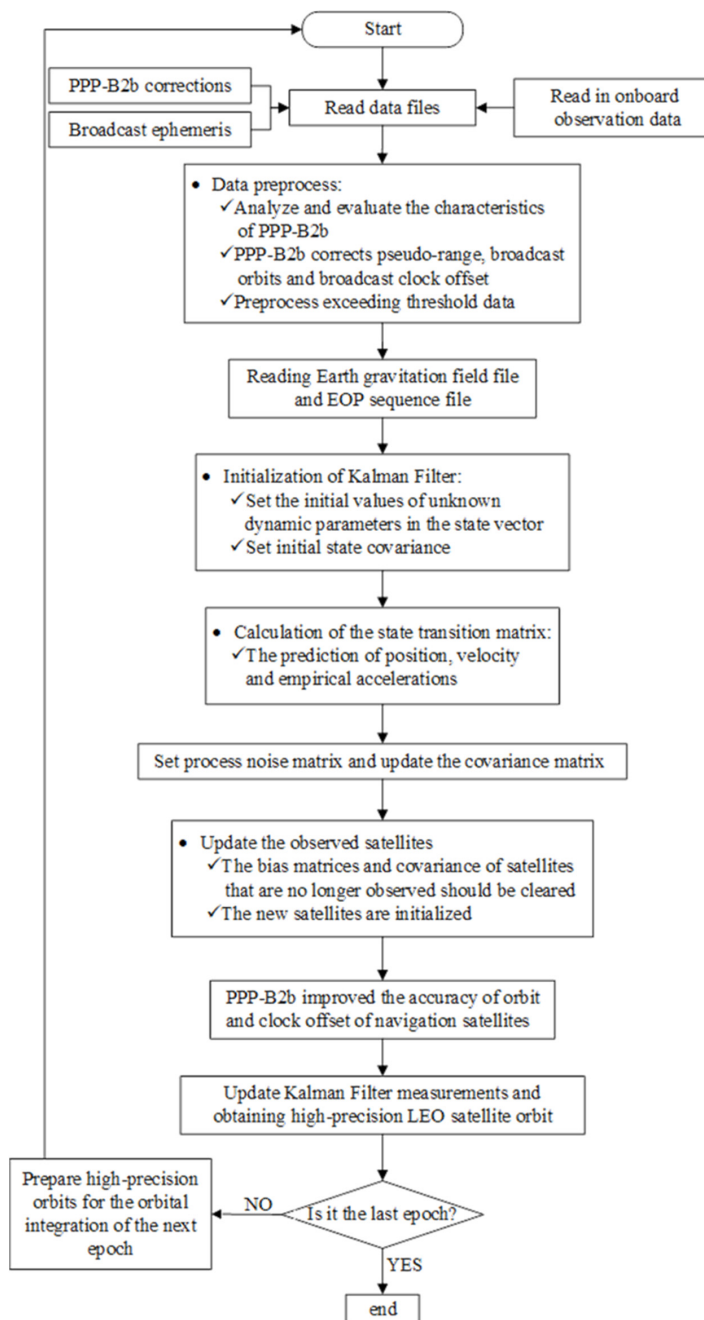
Type of Force	Model Adopted
Earth gravity model	EIGEN-6C ( $70 \times 70$ ) [22]
N-body disturbance	JPL DE405
Solid tide and pole tide	IERS 2010 [23]
Ocean tide	FES2014b [24]
Relative effect	IERS 2010 [23]
Solar radiation pressure	Macro Model [22]
Atmosphere drag	Harris–Priester density model, fixed area, estimating the drag parameter $C_D$ every 240 min [20]
Earth rotation parameter	Predicting EOP from Bulletin A in IERS2010 [23]
Empirical forces	Six piecewise periodical terms in the three (along, cross, and radial) directions, Cr and Sr represent radial periodical parameters, Ct and St represent that in the along direction, and Cn, Sn for the cross direction, estimated every 90 min

**Table 3.** GNSS data processing strategy for the TJU-01 satellite RT POD.

Items	Model Adopted
Observation model	Carrier-phase and pseudo-range undifferenced dual-frequency ionospheric-free combination
Cut-off elevation	1°
Processing arc	9-day arc
Sampling interval	1 s
Terrestrial frame	ITRF2020 [25]
Observation weight	$P = \sin e / \sigma^2$ . $\sigma^2$ represents the variance in code or carrier-phase measurements
Receiver clock offset	White noise estimation
Receiver ISB	Random walk process
Filtering method	Extended Kalman filter
Ambiguity parameter	Float solution

**Table 4.** Setting of parameters relating to processing noise.

Parameter	The Value of Initial Variance	The Value of Steady-State Variance	Correlation Time
LEO satellite position [m]	1.0	-	-
LEO satellite velocity [m/s]	1.0	-	-
GPS receiver clock offset [m]	500.0	50.0	1 s
ISB (G-C) [m]	1.2	1	1 s
Empirical force acceleration in radial direction [nm/s <sup>2</sup> ]	100.0	200.0	1 s
Empirical force acceleration in along direction [nm/s <sup>2</sup> ]	400.0	800.0	1 s
Empirical force acceleration in cross direction [nm/s <sup>2</sup> ]	200.0	400.0	1 s
Ambiguity parameter	0	0	1 s

**Figure 1.** Processing flow chart.

#### 4. Analysis and Evaluation of the PPP-B2b and Broadcast Ephemeris Performance

Before applying the PPP-B2b signals in the RT POD of LEO satellites, the statistical characteristics of the PPP-B2b corrections are analyzed and the RT orbit and clock offset accuracy of the PPP-B2b and broadcast ephemeris is evaluated.

##### 4.1. Analysis of the Characteristics of the PPP-B2b Correction Time Series

Taking a three-day dataset as an example, the PPP-B2b orbit and clock correction time series for the GPS (top) and BDS-3 (bottom) are shown in Figure 2. The GPS broadcast ephemeris (GPS LANV broadcast ephemeris) orbit errors and their PPP-B2b corrections in the along direction are the largest among the three axial directions of the centroid orbit coordinate system. Similarly, the BDS-3 medium Earth orbit (MEO) satellite orbit errors and their PPP-B2b corrections in the along direction are the largest among the three axial directions of the centroid orbit coordinate system. In addition, the broadcast ephemeris orbit errors and their PPP-B2b corrections are larger for the BDS-3 Inclined GeoSynchronous Orbit (IGSO) satellites than for the BDS-3 MEO satellites. A comparison of the different navigation systems reveals that the broadcast ephemeris orbit errors and their PPP-B2b corrections are smaller for the BDS-3 MEO satellites than for the GPS satellites. It is concluded from the above summary and Figure 2 that larger orbit errors and clock offset errors correspond to larger corrections and that the broadcast ephemeris errors positively correlate with the PPP-B2b corrections.

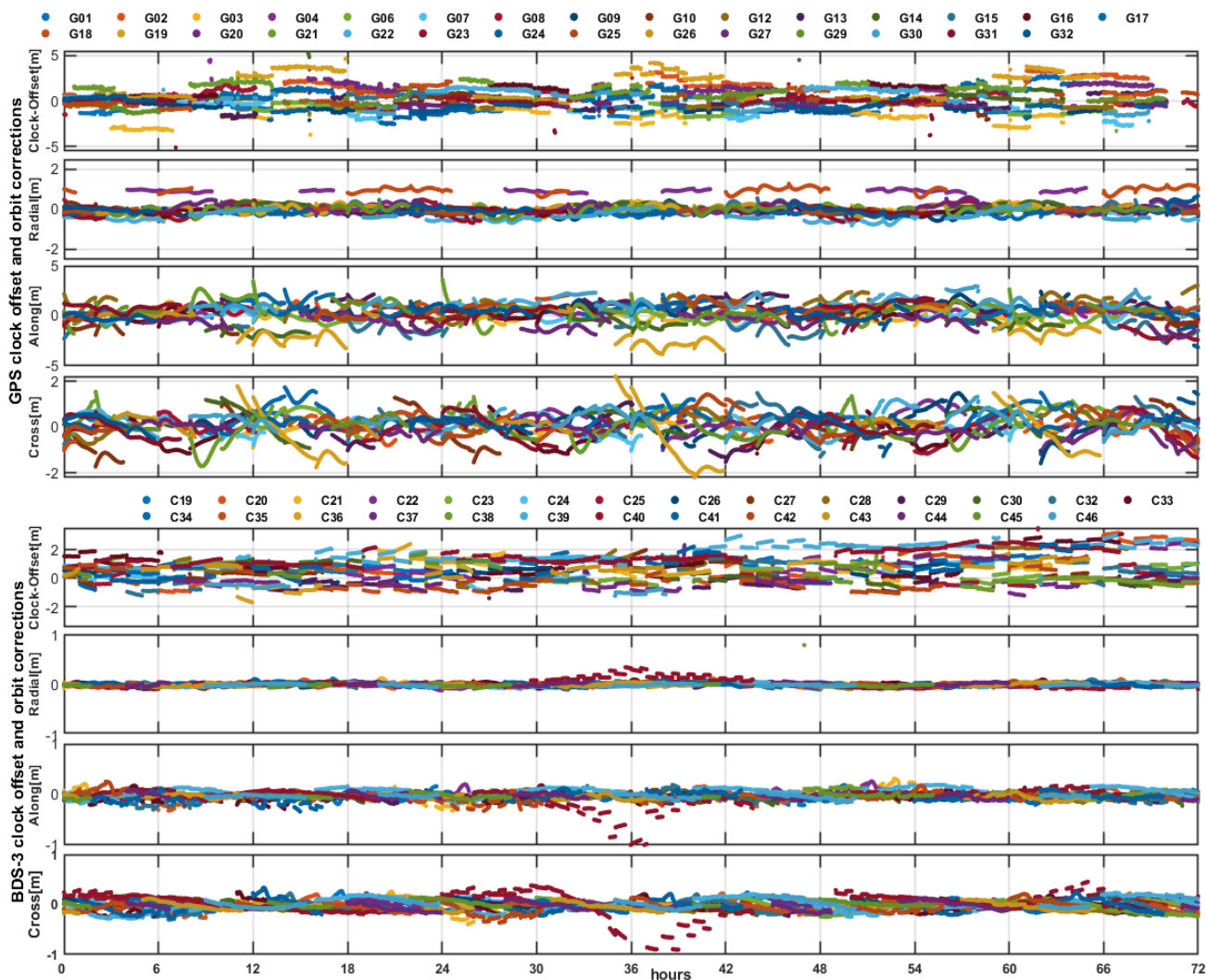


**Figure 2.** PPP-B2b correction time series.

#### 4.2. Evaluation of the PPP-B2b and Broadcast Orbit Accuracy

The final precision German Research Centre for Geosciences (GFZ) products are a reference for evaluating the accuracy of RT orbit determination [26]. The broadcast orbit reference point is the antenna phase center of the navigation satellite as for the PPP-B2b orbit whereas the GFZ precise orbit reference point is the centroid of the navigation satellite. Therefore, the IGS satellite antenna phase center offset correction file is used for eliminating the reference difference among the broadcast, PPP-B2b, and precise orbit. Figure 3 shows the GPS PPP-B2b and broadcast ephemeris orbit error series for a period of 3 days. The graph shows that after correction, the GPS satellite orbit errors in all three directions are not only smaller but also smoother, and the errors due to broadcast ephemeris update jumps are thus well compensated. The orbit errors in the along direction are the largest, and correspondingly, the correction in the along direction is the most obvious.

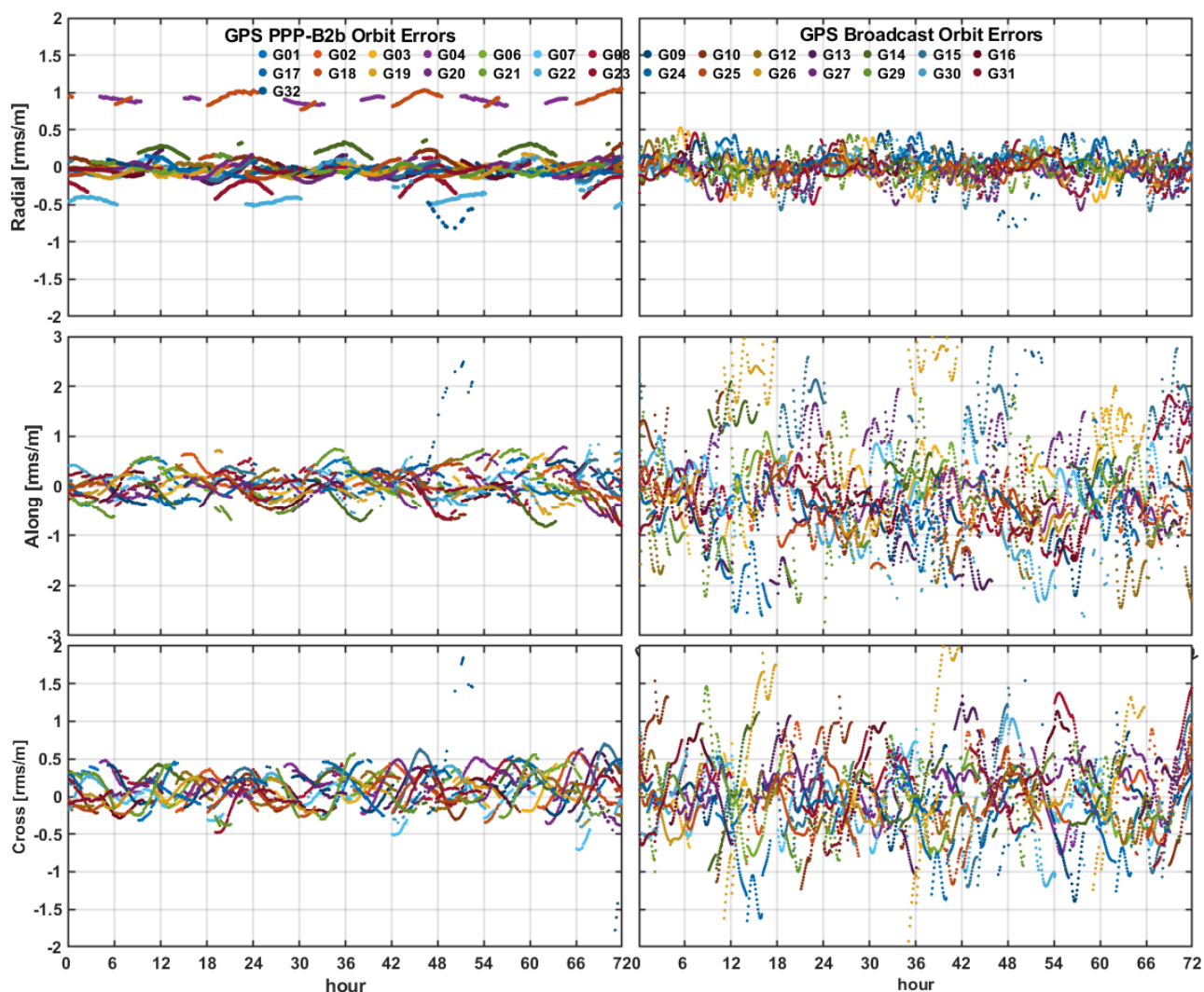


**Figure 3.** GPS orbit error series after PPP-B2b correction (left) and with the GPS broadcast ephemeris (right).

Figure 4 shows the PPP-B2b and broadcast ephemeris orbit error series for the BDS-3 MEO satellites. Overall, the PPP-B2b orbit errors of the BDS-3 MEO satellites are slightly smaller than the errors in the broadcast ephemeris. However, it is possible that the BDS-3 MEO PPP-B2b orbit precision is a little worse than the BDS-3 MEO broadcast ephemeris (BDS-3 CNAV1 broadcast ephemeris) orbit precision in some cases. It is thus possible to sacrifice some orbital numerical accuracy to make the orbit smoother and more continuous.

Therefore, the BDS-3 PPP-B2b orbit corrections not only slightly reduce the broadcast ephemeris orbit errors but also affect their discontinuity due to data updates.

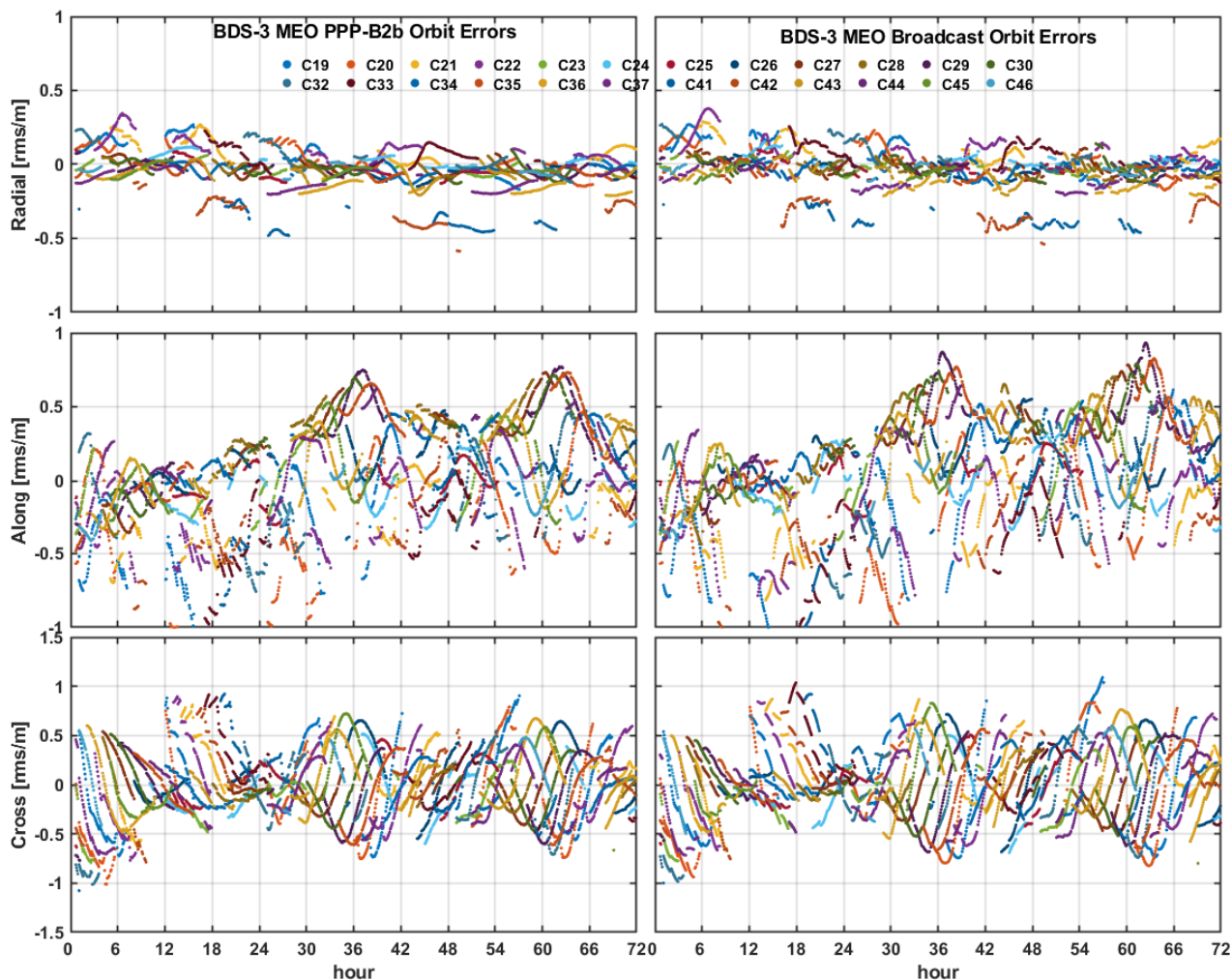


**Figure 4.** Orbit error series of BDS-3 MEO satellites after PPP-B2b correction (**left**) and with the original broadcast ephemeris (**right**).

Figure 5 shows the BDS-3 IGSO satellite broadcast ephemeris orbit error series with and without PPP-B2b correction. Similar to the case for the BDS-3 MEO satellites, after correction, the BDS-3 IGSO satellite broadcast ephemeris orbit errors are only slightly less but they are smoother. Figures 4 and 5 together reveal that the numerical precision of the broadcast orbit and PPP-B2b orbit of the BDS-3 IGSO satellite is much worse than that of the corresponding BDS-3 MEO satellite. This is due to only a few monitoring stations in specific areas receiving signals from the IGSO satellites, resulting in a poor geometric configuration when calculating the IGSO satellite broadcast ephemeris. The orbit accuracy of the IGSO satellites is thus lower than that of the MEO satellites.

To make an in-depth comparison of the orbit numerical precision between the PPP-B2b and broadcast ephemeris, the RMS errors of the PPP-B2b and broadcast ephemeris orbit are calculated for 9 days of data. The obtained orbit precisions are presented in Figure 6 and Table 5. The RMS errors of the GPS PPP-B2b orbit in the three axial directions of the centroid orbit coordinate system are 0.12 (radial), 0.34 (along), and 0.26 (cross) m, respectively. These values are much smaller than those of the GPS broadcast ephemeris, which are 0.17, 0.92, and 0.49 m in the corresponding directions. In summary, the GPS PPP-B2b clearly improves the GPS broadcast orbits. The same is observed for the BDS-3 satellites. The BDS-3 MEO satellite broadcast orbit is more accurate than that of the GPS satellite broadcast ephemeris.

as inter-satellite link observations are involved in the generation of the BDS-3 MEO satellite broadcast orbit [12]. It has been reported that the numerical precision of the BDS-3 satellite broadcast ephemeris orbit is currently much higher than that of 1 year ago, as the orbit accuracy is improving every 6 months.

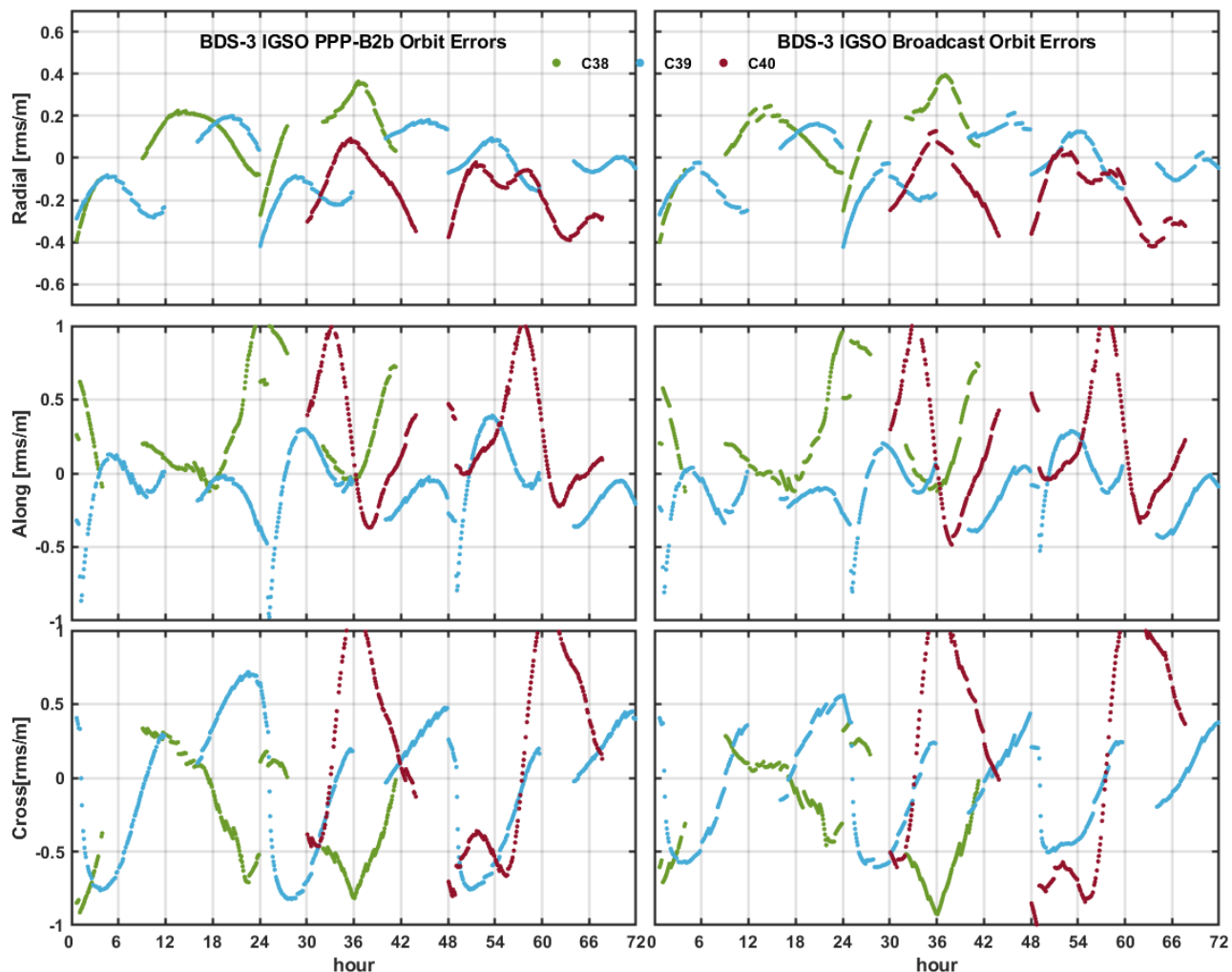


**Figure 5.** Orbit error series of BDS-3 IGSO PPP-B2b (left) and the BDS-3 IGSO broadcast ephemeris (right).

**Table 5.** Statistical accuracy of GPS and BDS-3 satellite orbits.

Ephemeris Type	MEO Orbit (RMS/m)			IGSO Orbit (RMS/m)		
	Radial	Along	Cross	Radial	Along	Cross
BDS broadcast ephemeris	0.11	0.31	0.28	0.17	0.34	0.47
BDS PPP-B2b	0.10	0.27	0.24	0.15	0.32	0.41
GPS broadcast ephemeris	0.17	0.92	0.49	-	-	-
GPS PPP-B2b	0.12	0.34	0.26	-	-	-

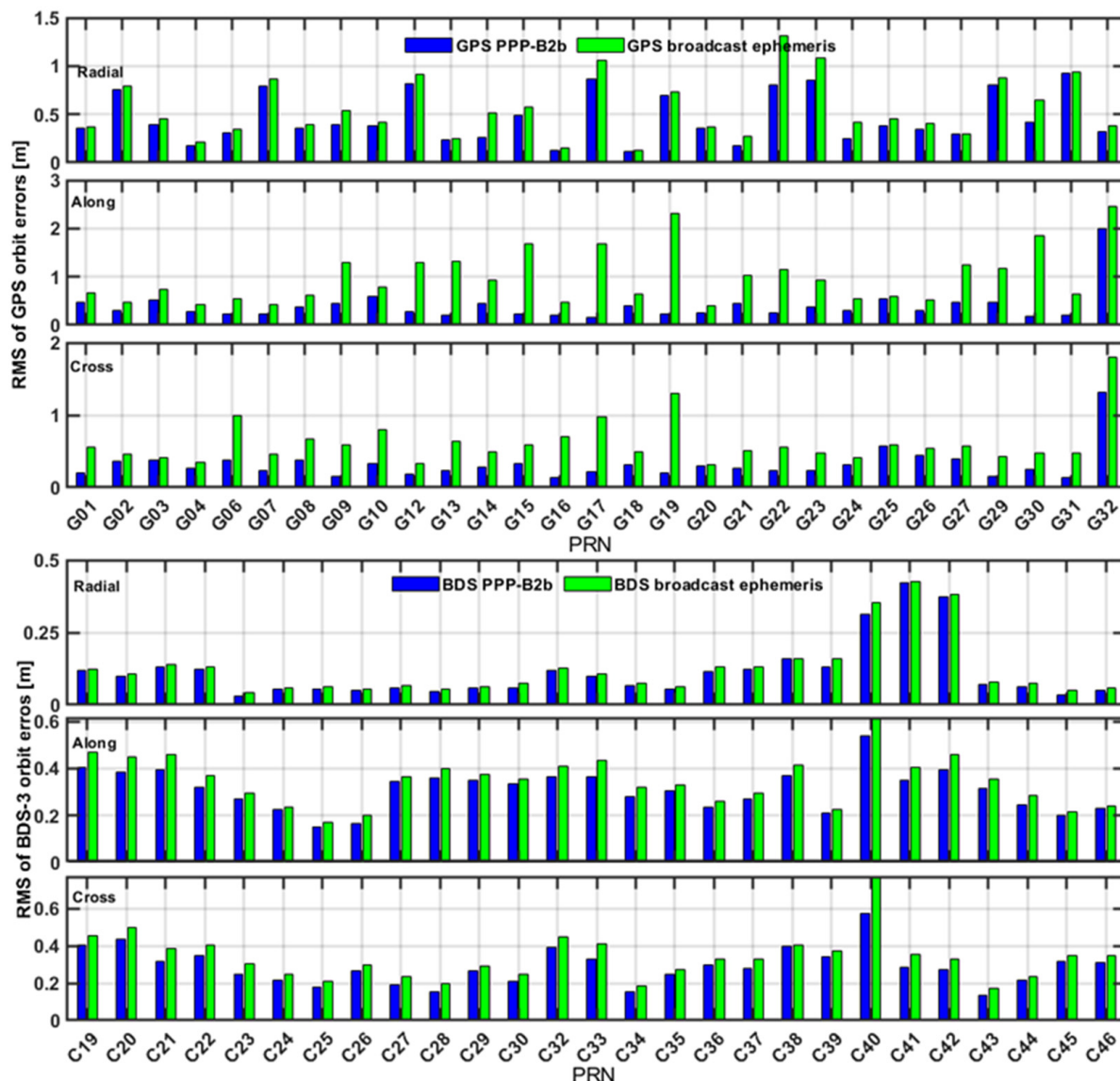


**Figure 6.** RMS errors in GPS satellite orbits (top) and BDS-3 satellite orbits (bottom).

#### 4.3. Evaluation of the RT Clock Offset Accuracy

The RT clock offset performance is assessed using the GFZ precise clock offset product as a reference. Before comparison, it is necessary to eliminate the reference time differences among the broadcast clock offset, PPP-B2b clock offset, and precise clock offset of the BDS-3 system using the time group delay and the DCB. We then select G32 and C40 as the reference satellite clocks for the GPS satellites and BDS-3 satellites, respectively, to make the time datum consistent between the broadcast clock offset and precise clock offset. The same method is applied to the PPP-B2b clock offset. The comparison results are presented in Figure 7.

Owing to the monitoring stations being distributed in small local areas, only part of the arc of the PPP-B2b clock correction is broadcast. In the case of the GPS PPP-B2b clock offset, there are jumps in the error at regular intervals that compensate for the large slips in the broadcast clock offsets resulting from the updating of the broadcast ephemeris. In addition, the broadcast clock offset errors are greater after correction, mainly because of systematic biases in the PPP-B2b corrections. Furthermore, system biases are included in the corrected clock offset. Although the BDS-3 PPP-B2b clock offsets also contain system biases, such systematic biases do not affect the RT POD accuracy. Figure 7 shows that the PPP-B2b clock offset errors tend to be more continuous and smoother than the errors of the

broadcast ephemeris, which effectively reduces the errors due to data updating. Owing to the systemic bias, the systematic STD is used in the evaluation of the nine-day clock offset datasets. All the evaluation results are shown in Figure 8. After correction, the STD obtained for the GPS PPP-B2b clock offset is 0.03 m, which is 50% less than that of the GPS broadcast clock offset. Similarly, the STD of the BDS-3 PPP-B2b clock offset is 6.8 cm, which is 70% less than that of the BDS-3 broadcast clock offset. Figure 7 shows that the errors in the GPS PPP-B2b clock offsets contain systematic biases and are much larger than those in the BDS-3 clock offsets. Aiming at reducing the effect of systematic biases in evaluating the PPP-B2b performance, a segmented statistics strategy is applied to the GPS PPP-B2b and broadcast clock offset errors. The GPS-PPP B2b and broadcast clock offset error series are divided into the several identical segments based on the GPS PPP-B2b clock offset error jump caused by the broadcast ephemeris update. The STD of each segment of the clock offset error for each satellite was calculated, then the average of these STDs of each satellite was calculated and the average of these STDs of all satellites was taken to obtain the STD of the entire satellite system at last. The resulting STDs of the GPS PPP-B2b offset errors are smaller than those of the BDS-3 PPP-B2b offset errors.

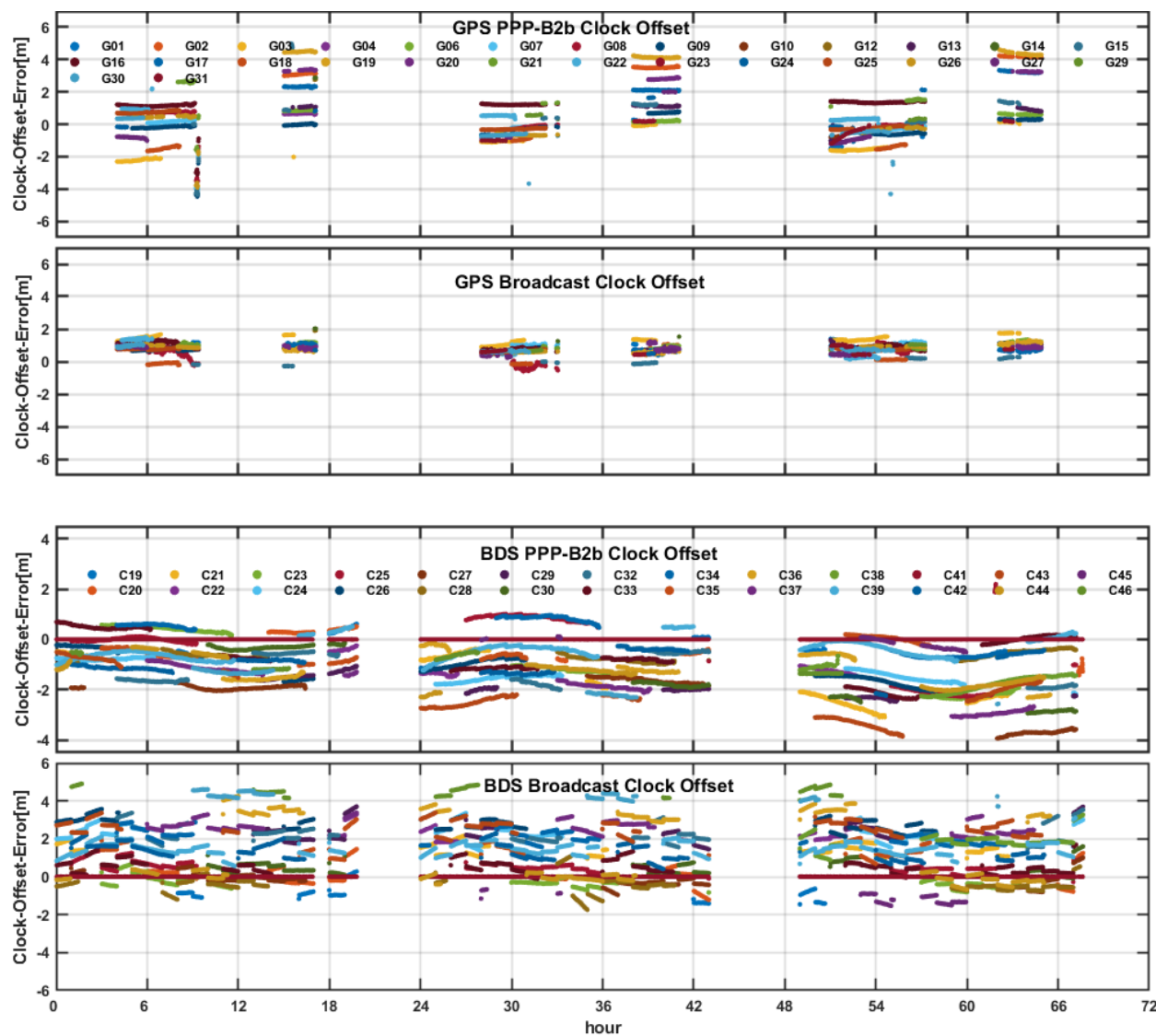


**Figure 7.** Error series in the GPS (top) and BDS-3 (bottom) broadcast clock offsets and PPP-B2b clock offsets.

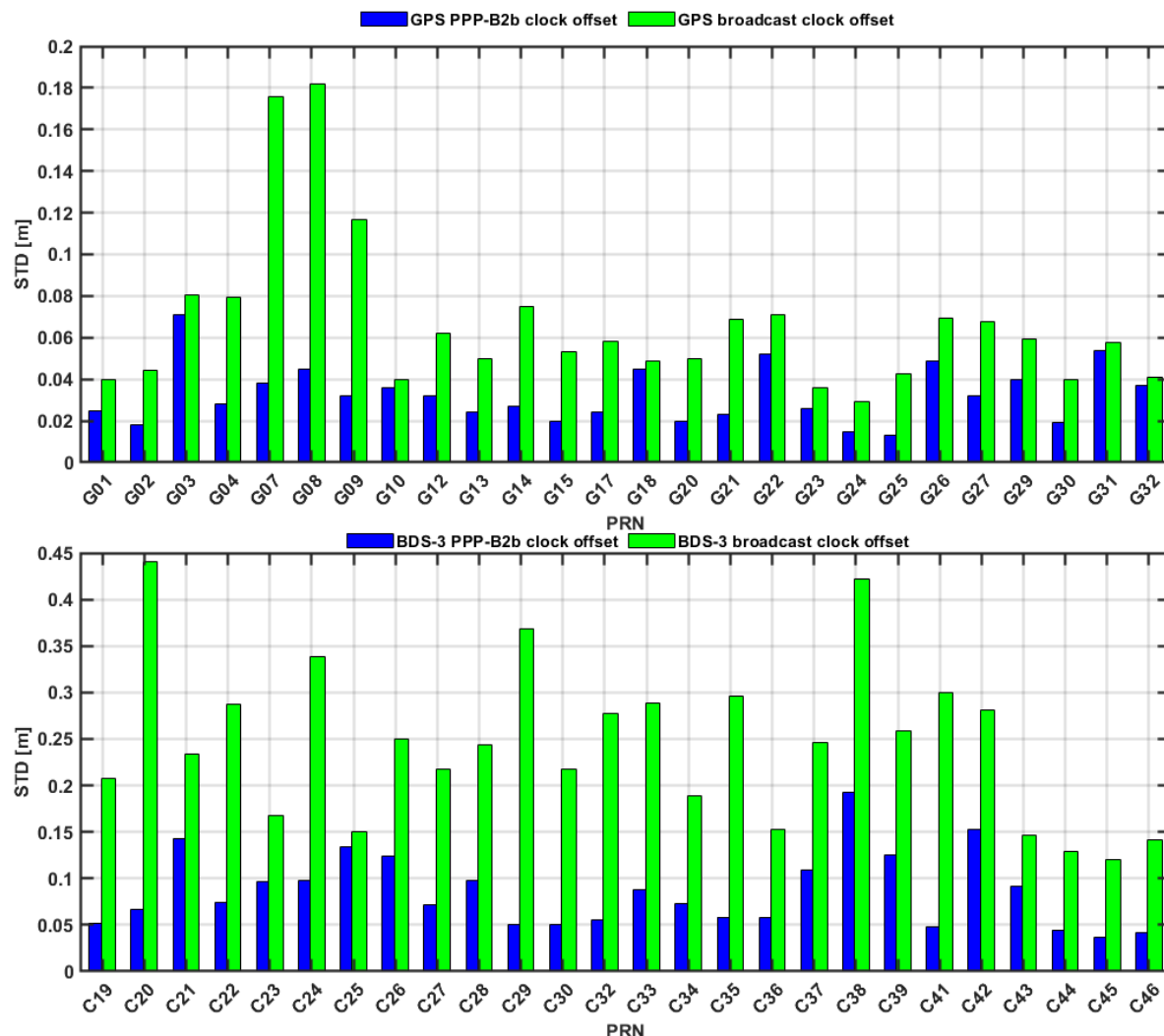


**Figure 8.** STDs of GPS and BDS-3 satellite clock offset errors with and without PPP B2b correction.

#### 4.4. Comparision of the Globally Averaged Signal in Space Range Error of PPP-B2b and Broadcast Empeheis

The signal in space in space range errors are more effective to characterize the common orbit and clock errors in the satellite-user directions. This article takes the signal in space range error (SISRE) as the key performance indicator of the system. According to Montenbruck Oliver and Xu xiaofei (2021) [27,28], the combined error of the radial orbit error and clock error  $\Delta RT$  can roughly characterize the globally averaged signal in space range error. The  $\Delta RT$ , SISRE, and SISRE (ORB) are calculated as follows:

$$\Delta RT = W_R \cdot \Delta X_{radial} - c \cdot \Delta t^s \quad (20)$$

$$SISRE_{orb} = \sqrt{[RMS(W_R \cdot \Delta X_{radial})]^2 + W_{A,C}^2 \cdot (A^2 + C^2)} \quad (21)$$

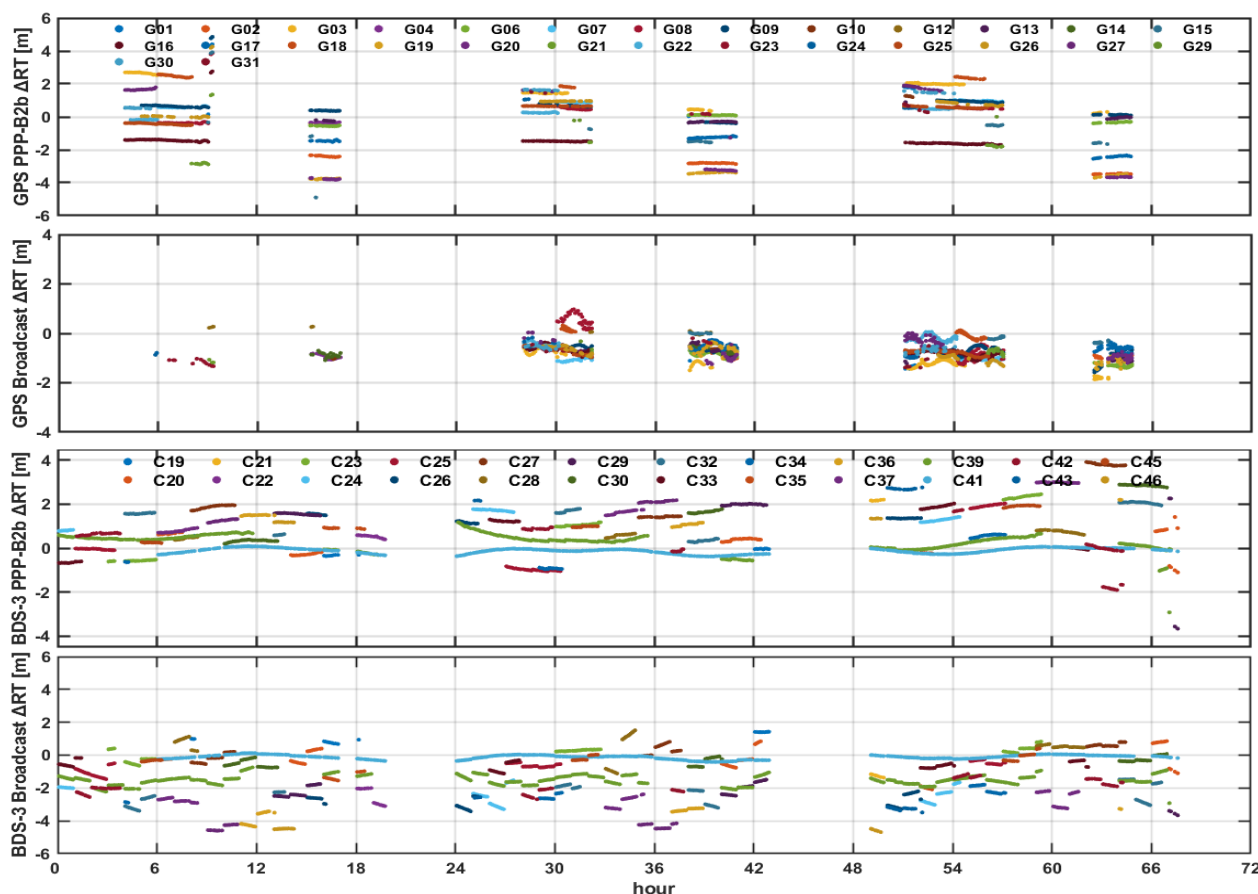
$$SISRE = \sqrt{[RMS(W_R \cdot \Delta X_{radial} - c \cdot \Delta t^s)]^2 + W_{A,C}^2 \cdot (A^2 + C^2)} \quad (22)$$

where  $W_R$  and  $W_{A,C}^2$  are the weight factors for the statistical contribution of radial (R), along-track (A), and cross-track (C) errors to the line-of-sight ranging error.  $\Delta X_{radial}$  is the orbit error in the radial direction;  $c$  represents the light speed in a vacuum; and  $\Delta t^s$  represents the clock offset error. A and C are the RMS of the orbit errors in the along and cross directions, respectively. The weight factors used for calculating the SISRE are shown in Table 6.

**Table 6.** The weight factors used for SISRE computation.

Ephemeris	Type	$W_R$	$W_{A,C}^2$
	GPS	0.98	1/49
	BDS-3 MEO	0.98	1/54
	BDS-3 IGSO	0.98	1/126

The GPS and BDS-3 PPP-B2b and broadcast ephemeris  $\Delta RT$  time series are shown in Figure 9. The RT series values of GPS PPP-B2b are larger than those of the broadcast ephemeris value, because there is a larger system bias in the GPS PPP-B2b clock offset error. After correction, the  $\Delta RT$  time series of the PPP-B2b and broadcast ephemeris are smoother than the broadcast ephemeris. Just like the clock offset series curve and orbit error series curve, the  $\Delta RT$  series also indicate that the PPP-B2b can reduce the effect caused by error jumps compared to the broadcast ephemeris.

**Figure 9.** Time series of  $\Delta RT$  for PPP-B2b and broadcast ephemeris.

The SISRE and SISRE (ORB) of the PPP-B2b and broadcast ephemeris are shown in Table 7. Compared to the GPS broadcast ephemeris, the SISRE (ORB) of GPS PPP-B2b has increased by 37.5% and the SISRE of GPS PPP-B2b has increased by 141.7%. Compared to the BDS-3 broadcast ephemeris, the SISRE (ORB) of BDS-3 PPP-B2b has increased by 29.8% and the SISRE of BDS-3 PPP-B2b has increased by 10.3%. It can be seen from Table 7 and the statistical data calculated above that after PPP-B2b correction, the accuracy of the GPS broadcast ephemeris and BDS-3 broadcast ephemeris have been improved significantly.

**Table 7.** The SISRE (ORB) and SISRE of the broadcast ephemeris and PPP-B2b.

Ephemeris	Type	SISRE (ORB)/m	SISRE/m
GPS broadcast		1.29	0.54
Ephemeris		0.81	0.22
GPS PPP-B2b		1.77	0.14
BDS-3 broadcast ephemeris		1.24	0.12
BDS-3 PPP-B2b			

## 5. RT POD Processing and Analysis

Firstly, the availability of the onboard GNSS observations of the TJU-01 satellite is analyzed. The visibility of the GPS and BDS-3 PPP-B2b signals is plotted and analyzed. The PPP-B2b improvement in the RT POD of the TJU-01 satellite is verified.

### 5.1. Availability Analysis of Onboard GNSS Data

High-quality GNSS onboard observations are required for the accurate RT POD of LEO satellites. In this subsection, the availability of onboard GNSS observations made on 31 January 2022 is analyzed as an example. The onboard GNSS receiver on the TJU-01 satellite tracks all GPS satellites and 33 BDS-2/3 satellites. The receiver channels are assigned to 5 GEO satellites including C01–C05, 7 IGSO satellites including C06–C16, and 22 MEO satellites including C11, C12, C14, C19–C30, and C32–C37. The sampling interval is 1 s. Approximately 8 GPS satellites and 12 BDS satellites only are tracked in the same epoch owing to the limited number of navigation channels. The undifferenced ionosphere-free pseudo-range and carrier-phase combination model used in this study requires GPS/BDS dual-frequency phase and code measurements at each epoch. Here, the data availability of the satellite is defined as the ratio of the number of epochs with complete dual-frequency observations to the total number of epochs for that satellite. The data availability of the observations of the TJU-01 satellite is analyzed as follows. Figure 10 shows that the availability of GPS observations is clearly lower than that of the BDS observations, which may lead to the RT POD having a lower accuracy when using the GPS than when using the BDS.

### 5.2. Availability of PPP-B2b in the RT POD of the TJU-01 Satellite

This study assumes that the TJU-01 satellite can receive PPP-B2b signals. The sampling interval for the TJU-01 satellite observations used in the visibility analysis is 30 s. The TJU-01 satellite observation onboard GNSS receiver can track 8 GPS satellites and 12 BDS satellites, including BDS-2 and BDS-3. Owing to the restricted distribution of monitoring stations, PPP-B2b can only provide corrections of flight arcs over the Asia-Pacific region for the BDS-3 and GPS satellites. Considering the high speed of LEO satellites, their geometric configuration with GEO will constantly change. When the Earth is located on the line connecting GEO and LEO satellites, it will obstruct the signal of GEO satellites, and LEO satellites will not be able to receive the PPP-B2b correction. The availability and visibility of PPP-B2b are computed and plotted for the TJU-01 satellite at each epoch on 31 January 2022, as shown in Figures 11 and 12 and Table 8 (GPS) and Table 9 (BDS-3). Figure 11 presents the number of satellites that can receive PPP-B2b corrections at each epoch corresponding to the sub-satellite point trajectory of the TJU-01 satellite. Up to eight GPS satellites can receive PPP-B2b corrections at a certain epoch, whereas up to seven BDS-3 satellites can receive the PPP-B2b correction.

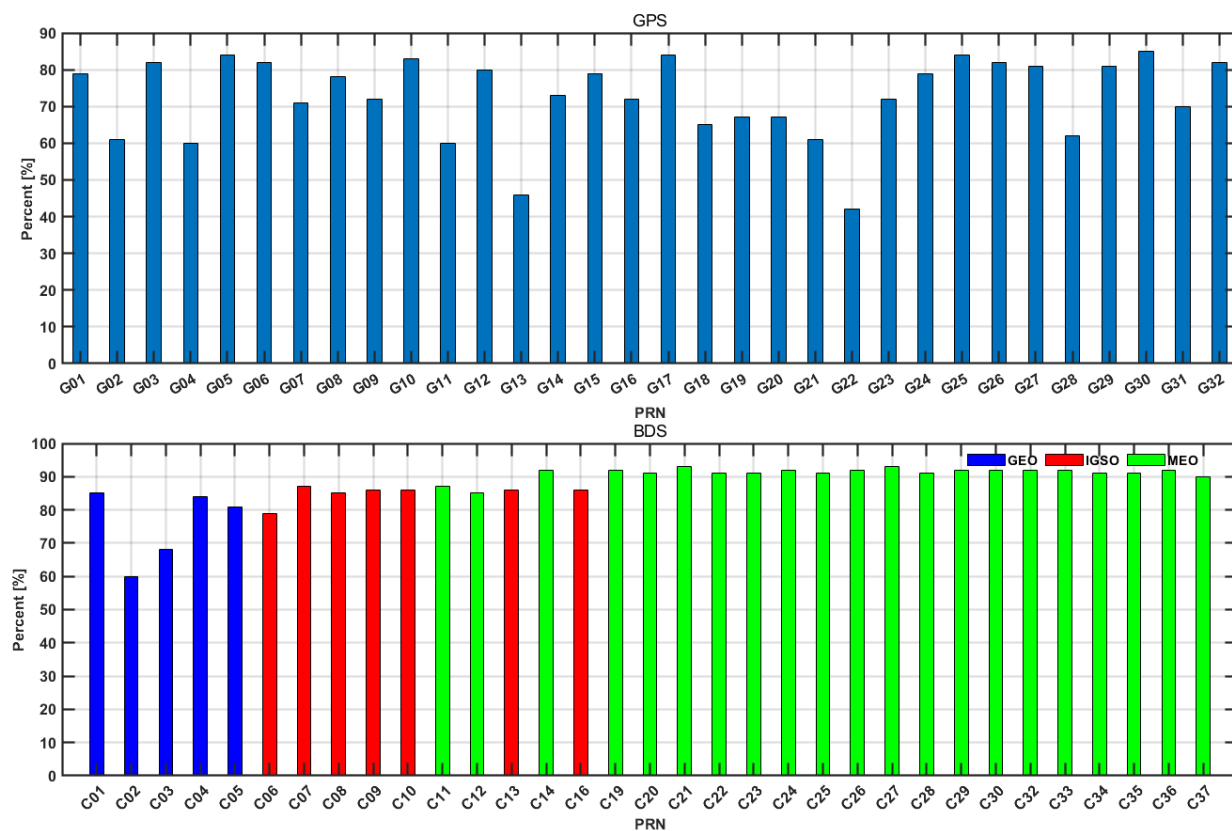


**Figure 10.** Data availability rate of the GPS (**top**) and BDS (**bottom**) observations onboard the TJU-01 satellite.

**Table 8.** Statistical availability of the GPS PPP-B2b for the TJU-01 Satellite.

Number of Satellites	0	1	2	3	4	5	6	7	8
Available epochs	800	471	475	450	223	177	79	33	3
Total number of GPS satellites	6400	3768	3800	3600	1784	1416	632	264	24
Epoch proportion (%)	29.5	17.4	17.5	16.5	8.2	6.5	2.9	1.2	0.1
Quantity proportion (%)	0	12.5	25	37.5	50	67.3	75	87.3	100

**Table 9.** Statistical availability of PPP-B2b for the TJU-01 satellite.

Number of Satellites	0	1	2	3	4	5	6	7
Available epochs	338	543	462	520	436	291	68	2
Total number of BDS3 satellites	2628	4071	3493	3981	3334	2209	500	21
Epoch proportion (%)	12.7	20.3	17.3	19.5	16.3	10.9	2.5	0.1
Quantity proportion (%)	0	13.3	26.5	39.2	52.3	65.9	81.6	66.7

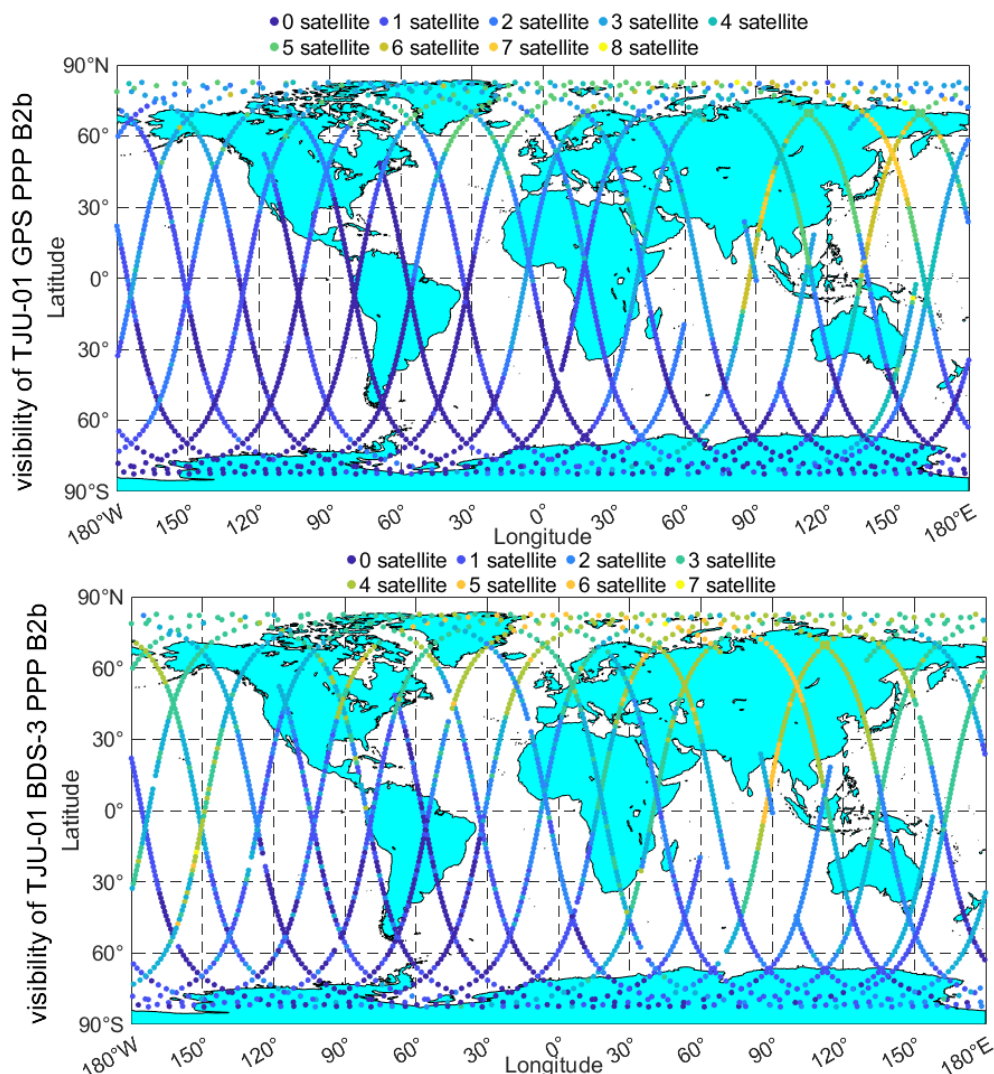


**Figure 11.** Sub-satellite point trajectory of the TJU-01 satellite with available numbers of GPS PPP-B2b (**top**) and BDS PPP-B2b (**bottom**) corrections.

Figure 12 shows the percentages of the GPS and BDS-3 satellites receiving corrections relative to the number of satellites observed by the TJU-01 satellite at each epoch on a single day. It is seen that compared with the signals observed by ground stations, the PPP-B2b signals observed by BDS-3 and the GPS have a wider geographical range. The geographical range in which PPP-B2b is received by the GPS and BDS-3 navigation systems is much larger than the geographical range of ground stations, mainly because the TJU-01 satellite is much higher than the ground stations.

The percentage GPS reception is smaller than the percentage BDS-3 reception for two main reasons. Firstly, fewer GPS satellites than BDS-3 MEO satellites receive the PPP-B2b signals. This mainly results from the different configurations of the GPS and BDS-3 satellite constellations. Secondly, more GPS satellites than BDS-3 satellites are observed by the TJU-01 satellite at each epoch.

Figures 11 and 12 reveal that except over the southeastern Pacific, southwestern Atlantic, and South America, the TJU-01 satellite receives PPP-B2b signals from above most parts of the world. The main receiving area of the PPP-B2b signal for the TJU-01 satellite is over the Chinese mainland.

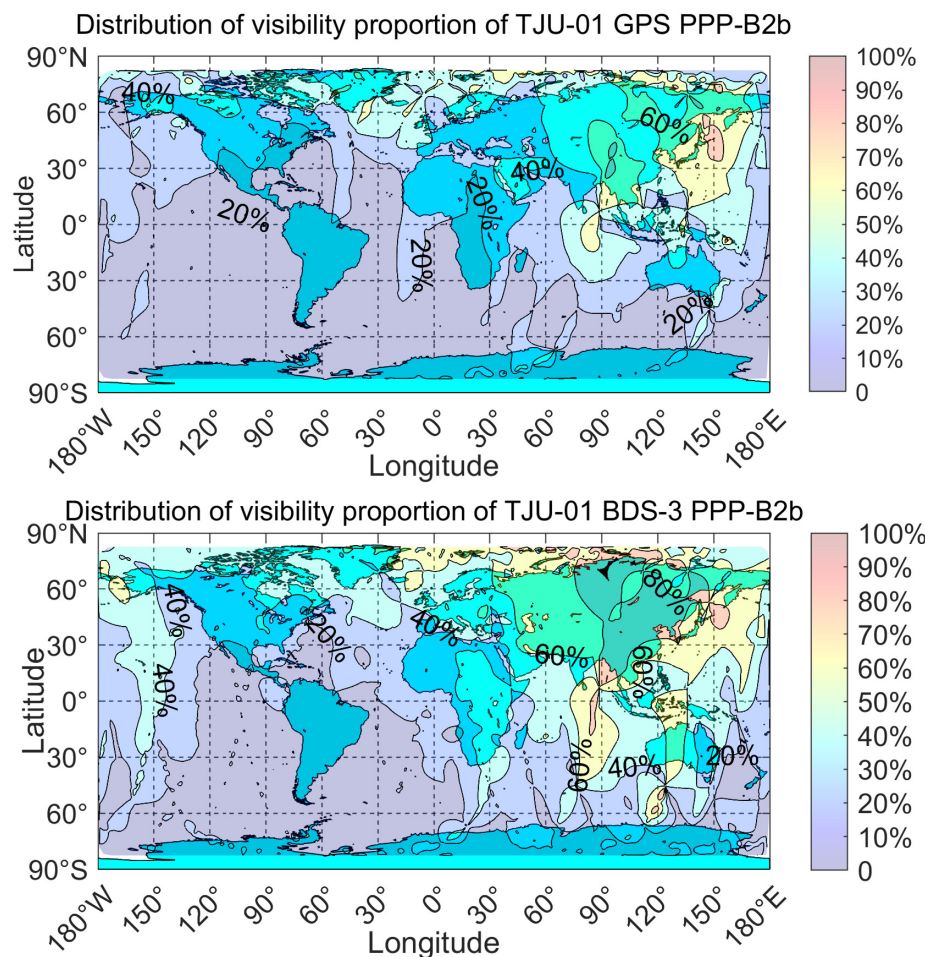


**Figure 12.** Distribution of the proportion of PPP-B2b signal visibility from the TJU-01 satellite.

The detailed statistical availability of the GPS PPP-B2b for the TJU-01 satellite is given in Table 8. The valid number of GPS observations of the TJU-01 satellite is 2711 epochs. The number of satellites observed is 20,237, and the number of PPP-B2b corrections received is 5253. The numbers of epochs receiving different numbers of corrections are given in Table 8. The epochs receiving PPP-B2b account for 70.5% of all epochs. The epochs receiving more than three PPP-B2b corrections account for nearly 35% of all epochs. The number of PPP-B2b corrections received by the TJU-01 satellite exceeds 50% of the number of satellites observed at the same epoch account in nearly 19% of all epochs. Relative to the GPS broadcast ephemeris, the GPS PPP-B2b at these observed epochs should improve the accuracy of the RT POD of the TJU-01 satellite.

The detailed statistical availability of the BDS-3 PPP-B2b for the TJU-01 satellite is given in Table 9. The valid number of observations of the TJU-01 satellite is 2667 epochs. The number of satellites observed is 20,295, and the number of PPP-B2b corrections received is 6669. The epochs receiving PPP-B2b account for 87.3% of all epochs. The epochs receiving PPP-B2b corrections account for nearly 50% of all epochs. The number of PPP-B2b corrections received by the TJU-01 satellite exceeds 50% of the number of epoch satellites in nearly 30% of all epochs. Relative to the BDS-3 broadcast ephemeris, the BDS-3 PPP-B2b at these observed epochs improves the accuracy of the RT POD of the TJU-01 satellite.

Figures 11 and 12 and Tables 8 and 9 reveal that compared with the case for the BDS-3 satellites, the GPS satellites receive PPP-B2b data over a smaller geographical range. There are two main reasons. (1) The constellation configurations are different. The MEO satellites of BDS-3 are higher than the GPS satellites, which allows the TJU-01 satellite to monitor the BDS-3 MEO satellite flying over the Asia-Pacific region for longer. (2) Owing to the smaller number of signal channels, the GPS observation data integrity is lower than that of

the BDS-3 observation data, resulting in fewer available GPS PPP-B2b corrections and a smaller geographical range of reception for the GPS PPP-B2b. These differences may result in the different accuracy of the RT POD of the TJU-01 satellite.

### 5.3. Results and Analysis of the RT POD of the TJU-01 Satellite

In this study, the RT POD of the TJU-01 satellite is performed in a simulated mode based on real onboard observations considering PPP-B2b signals. The post-POD solutions with a precise orbit and clock offset from GFZ are used for reference to assess our RT POD performance. The post-processed orbits overlap differences of TJU-01 are 2–3 cm in the radial, along, and cross directions from January 28 to 5 February 2022. In an effort to test the enhancement effect of PPP-B2b on the RT POD of LEO satellites, the results of the RT POD of the TJU-01 satellite on 31 January 2022 are compared, as presented in Figure 13, for the GPS PPP-B2b versus the GPS broadcast ephemeris, the BDS-3 PPP-B2b versus the BDS-3 broadcast ephemeris, and the GPS and BDS-3 PPP-B2b versus the GPS and BDS-3 broadcast ephemeris.

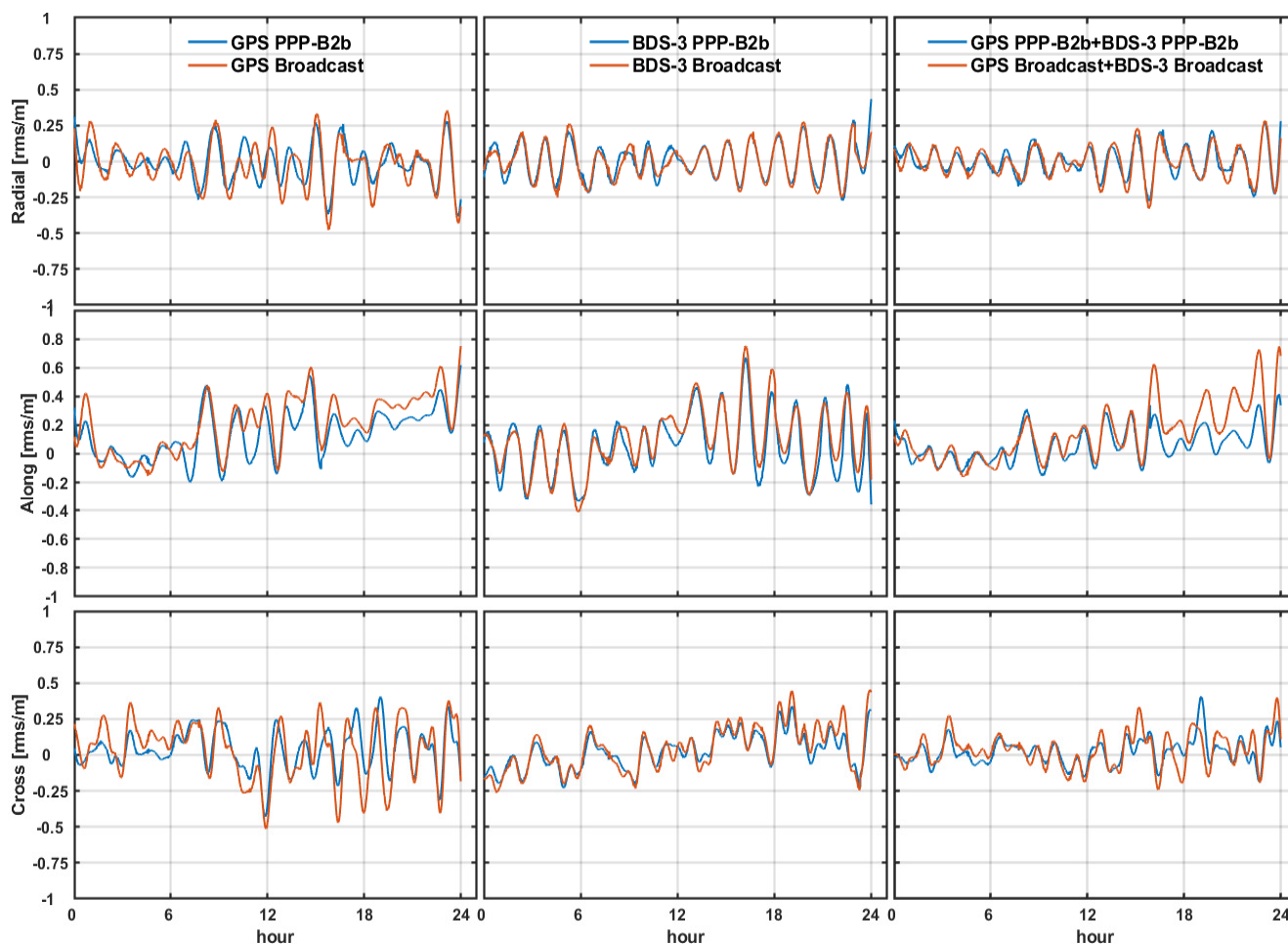


**Figure 13.** Comparison of error series of the RT POD of the TJU-01 satellite using the PPP-B2b and broadcast ephemeris.

Figure 13 reveals that PPP-B2b improves the RT POD accuracy of the TJU-01 satellite. The RT POD errors when using PPP-B2b are smaller than those when using the broadcast ephemeris. Meanwhile, the navigation satellite orbit errors and TJU-01 satellite's RT POD errors in the along direction are the largest among the three directions. It is thus concluded that the orbit errors of the navigation satellites and the RT POD errors of the LEO satellites are positively correlated. To further assess the improvement effect of PPP-B2b on the RT

POD of the TJU-01 satellite, the 9-day results are compared and averaged in Figure 14 and Table 10. Figure 14 shows that the TJU-01 satellite RT POD errors decrease the most in the along direction among the three directions, as PPP-B2b has the greatest correction in the along direction for the navigation satellite orbit errors.

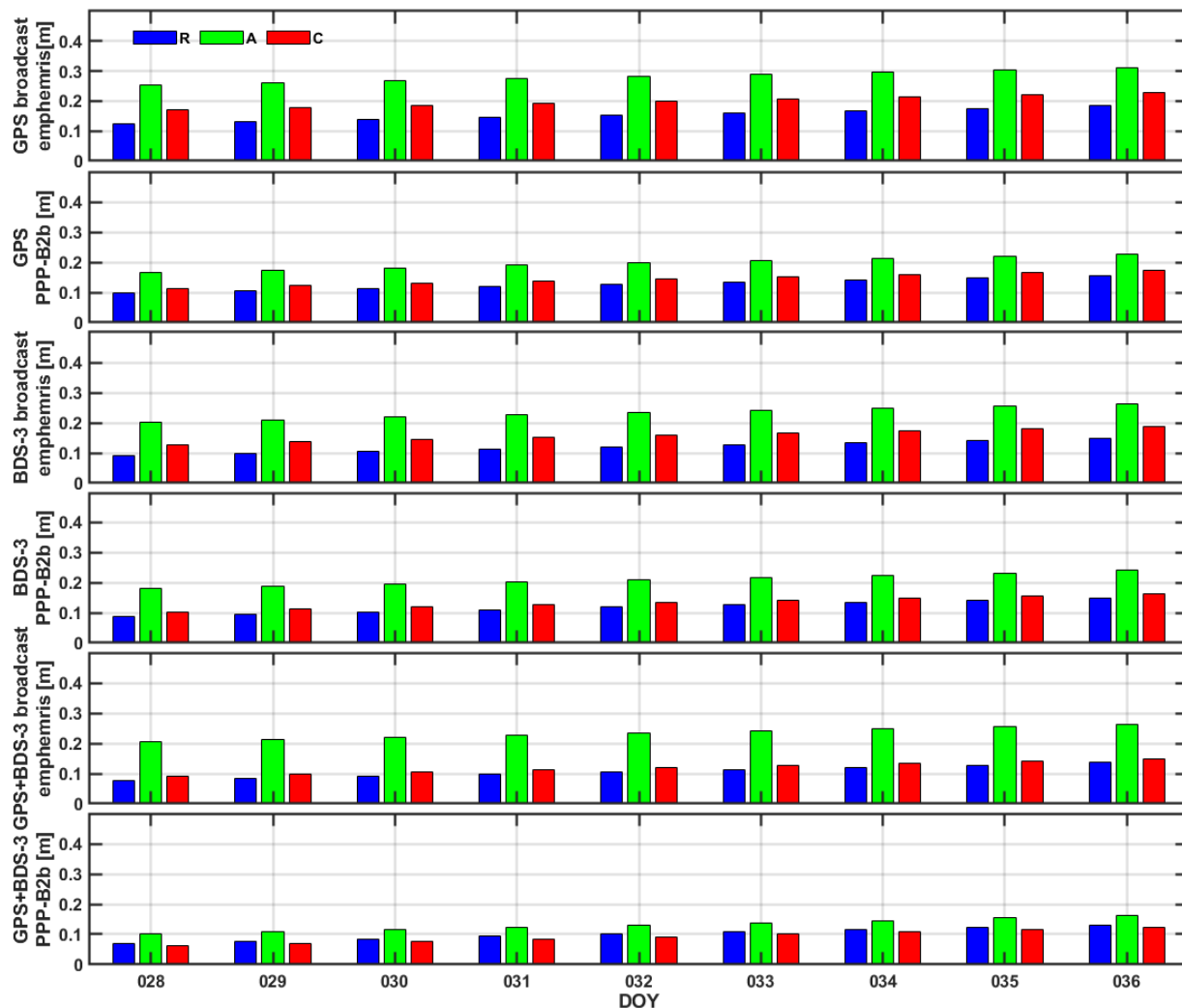


**Figure 14.** Comparison of the RMS of the orbit errors in radial, along, and cross directions for the RT POD of the TJU-01 satellite.

**Table 10.** Comparison of the results of the RT POD of the TJU-01 satellite between the use of the broadcast ephemeris and PPP-B2b.

Ephemeris	Direction	Radial (RMS/m)		Along (RMS/m)		Cross (RMS/m)	
		Not Corrected	B2b Corrected	Not Corrected	B2b Corrected	Not Corrected	B2b Corrected
GPS broadcast ephemeris		0.15	0.12	0.28	0.19	0.19	0.14
BDS-3 broadcast ephemeris		0.12	0.11	0.23	0.20	0.16	0.13
GPS + BDS-3 broadcast ephemeris		0.11	0.10	0.21	0.13	0.12	0.09

Table 10 shows that the accuracy of the RT POD of the TJU-01 satellite is higher when using the BDS-3 broadcast ephemeris than when using the GPS broadcast ephemeris and higher when using the BDS-3 PPP-B2b than when using the GPS PPP-B2b. The reasons are

as follows. (1) Owing to the inter-satellite links, the BDS-3 broadcast orbit accuracy is higher than the GPS broadcast orbit accuracy. (2) More BDS-3 satellites than GPS satellites receive PPP-B2b. (3) The integrity of GPS observations is worse than that of BDS-3 observations. Furthermore, the most accurate scheme is using GPS and BDS-3 PPP-B2b for the RT POD of the TJU-01 satellite, as there are more onboard observation GNSS data and more navigation satellites receiving PPP-B2b corrections.

#### 5.4. Correlation Analysis of PPP-B2b Reception Ratio and Accuracy Improvement Ratio

The correlation between  $R_r^N$  given by Equation (23) and  $\delta$  given by Equation (24) is next analyzed, where  $R_r^N$  is the ratio of the number of navigation satellites receiving PPP-B2b corrections to the number of navigation satellites observed at a certain epoch. The superscript  $N$  indicates the navigation system.  $N = G$  indicates the GPS whereas  $N = C$  indicates the BDS. The subscript  $r$  represents reception.  $NUM_{B2b}$  is the number of PPP-B2b corrections that the TJU-01 satellite receives at a certain epoch for a certain navigation system whereas  $NUM_{all}$  is the number of the navigation satellites observed by the TJU-01 satellite at the same epoch.  $\delta$  is the percentage improvement, due to PPP-B2b, in the accuracy of the RT POD of the TJU-01 satellite relative to the broadcast ephemeris.  $S_{Broad}$  and  $S_{B2b}$  are the RT POD errors for the TJU-01 satellite when using the broadcast ephemeris and PPP-B2b for navigation system  $N$  in the three orthogonal directions at a certain epoch. Minor gross errors in  $\delta$  are removed, and  $\delta$  time series are then fitted and smoothed. The time series of  $R_r^N$  and  $\delta$  over the course of one day are shown in Figure 15. It is seen that a larger  $\delta$  corresponds to a greater improvement in the PPP-B2b orbit determination accuracy. We have

$$\delta = \frac{S_{Broad} - S_{B2b}}{S_{B2b}} \quad (23)$$

$$R_r^N = \frac{NUM_{B2b}}{NUM_{all}} \quad (24)$$

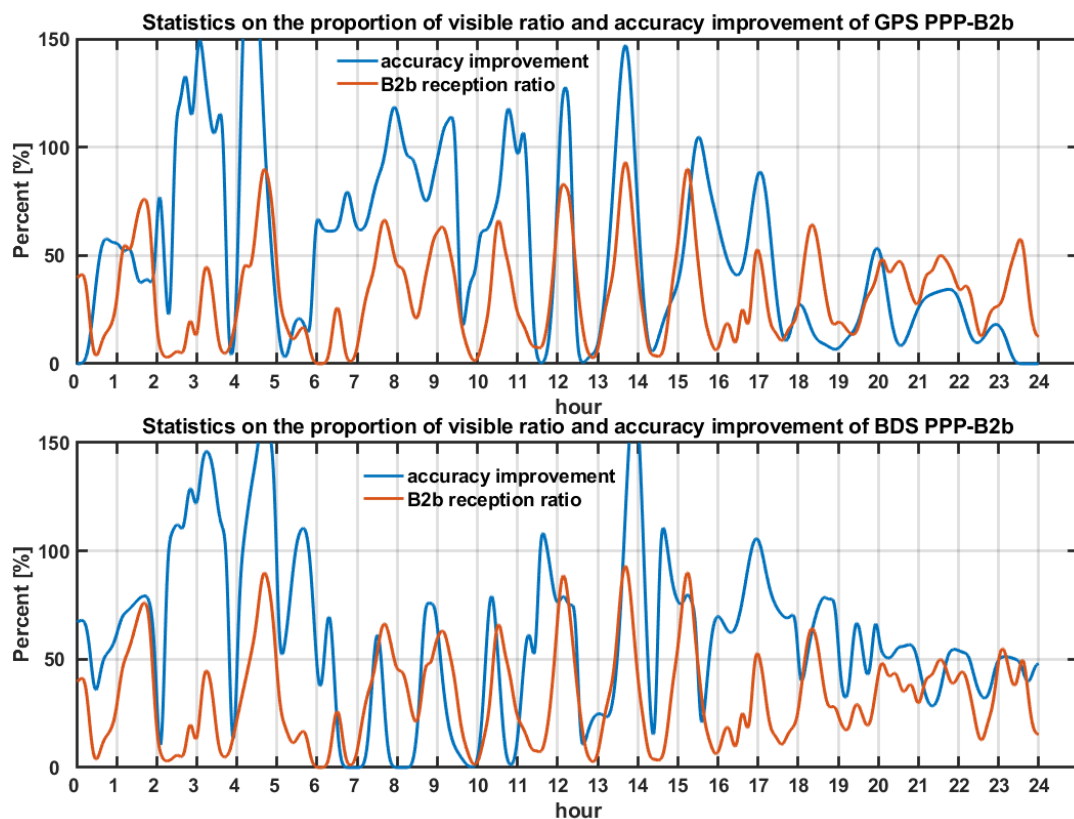


**Figure 15.** Correlation analysis of the PPP-B2b reception ratio and accuracy improvement ratio.

Figure 15 shows that  $R_r^N$  and  $\delta$  are positively correlated. As the proportion of PPP-B2b corrections received increases, the improvement in the accuracy of the RT POD of the TJU-01 satellite using PPP-B2b increases. However, the correlation between the GPS PPP-B2b reception ratio and accuracy improvement ratio is slightly different from that for the BDS-3. This is mainly due to the different missing observation epochs between the GPS and BDS-3 in the TJU-01 satellite observations and the interpolation of  $R_r^N$  and  $\delta$  in the different missing, thus causing correlation differences. In addition, for the same reception ratio, different numbers of GPS and BDS-3 satellites are observed by the TJU-01 satellite. As the numbers of GPS and BDS-3 satellites that can receive PPP-B2b are different, there are differences in the improvement in the observation accuracy. Therefore, there are differences between the GPS and BDS-3 in the correlation between the PPP-B2b reception ratio and accuracy improvement ratio.

## 6. Conclusions

The following conclusions are drawn from the results of this study.

1. The RMS of the GPS broadcast ephemeris orbit errors in the along direction (0.92 m) is greater than that in the radial direction (0.17 m) and that in the cross direction (0.49 m). In addition, errors in the along direction are corrected most by the GPS PPP-B2b (by approximately 60%) among the three directions. The RMS of the GPS PPP-B2b orbit errors in the radial, along, and cross directions is 0.12, 0.34, and 0.26 m, respectively.
2. For BDS-3, the orbit errors of PPP-B2b are a few centimeters smaller than those of the broadcast ephemeris. The orbit errors of the IGSO satellite broadcast ephemeris are much greater than those of the MEO satellite broadcast ephemeris, and the orbit correction of the IGSO satellites is greater than the orbit corrections of the MEO satellites. The RMS of the MEO satellite PPP-B2b orbit errors in the radial, along, and cross directions is 0.10, 0.27, and 0.24 m, which is better than those of the IGSO satellites, 0.15, 0.32, and 0.41 m, respectively.
3. PPP-B2b correction improves the broadcast clock offset accuracy remarkably. For BDS-3, the average value of the STDs of the PPP-B2b clock offset is approximately 0.07 m. The accuracy is 70% higher than that of the broadcast ephemeris clock offset. For the GPS, the average value of the STDs of the PPP-B2b clock offset is approximately 0.03 m, i.e., the accuracy is 50% better than that of the broadcast ephemeris clock offset.
4. The smoothness and continuity of the navigation satellite orbit and clock offset error series are improved by the PPP-B2b service, which reduces the errors introduced by broadcast ephemeris data updates.
5. As the TJU-01 satellite is much higher than ground stations, it has a wider geographical range of PPP-B2b reception. Up to eight GPS satellites can receive the PPP-B2b correction at a certain epoch whereas up to seven BDS-3 satellites can receive the PPP-B2b correction.
6. More BDS-3 satellites than GPS satellites can receive PPP-B2b. The BDS-3 and GPS satellite constellations have different configurations, and the integrity of the GPS observations is lower than that of the BDS-3 observations.
7. As PPP-B2b mainly reduces errors in the broadcast ephemeris orbit in the along direction, the errors in the RT POD of the TJU-01 satellite using PPP-B2b in the along direction are smaller than those when using the broadcast ephemeris.
8. The accuracy of the RT POD of the TJU-01 satellite when using the GPS broadcast ephemeris is lower than that when using the BDS-3 broadcast ephemeris because the inter-satellite links improve the accuracy of the BDS-3 broadcast ephemeris, and more BDS-3 satellites than GPS satellites receive PPP-B2b. Moreover, the integrity of the GPS observations is lower than that of the BDS-3 observations.
9. The most accurate scheme is using the GPS and BDS-3 PPP-B2b for the RT POD of the TJU-01 satellite. The accuracy is improved by 5.1%, 43.9%, and 28.7%, respectively, in the radial, along, and cross directions relative to using the GPS and BDS-3 broadcast ephemeris.

10. As the proportion of PPP-B2b correction reception increases, the accuracy improvement of PPP-B2b in the RT POD of the TJU-01 satellite increases.

**Author Contributions:** Conceptualization, M.L. and T.X.; methodology, Y.S.; software, Y.S. and K.W.; validation, Y.S. and S.W.; formal analysis, Y.S.; investigation, M.L. and T.X.; resources, M.L. and T.X.; data curation, Y.S.; writing—original draft preparation, Y.S.; writing—review and editing, M.L. and T.X.; visualization, S.W. and D.W.; supervision, M.L. and T.X.; project administration, M.L. and T.X.; funding acquisition, M.L. and T.X. All authors have read and agreed to the published version of the manuscript.

**Funding:** This research was funded by the National Natural Science Foundation of China (Grant No. 42204015), National Key Research and Development Program of China (2020YFB0505800 and 2020YFB0505804), and the Natural Science Foundation of Shandong Province (ZR2022QD094).

**Data Availability Statement:** The multi-GNSS precise clock and orbit products can be accessed at <ftp://igs.ign.fr/pub/igs/products/mgex/> (accessed on from 28 January 2022 to 5 February 2022), the GPS LANV broadcast ephemeris can be achieved at <ftp://igs.gnsswhu.cn/pub/gps/data/daily/> (accessed on from 28 January 2022 to 5 February 2022), the BDS-3 CNAV1 broadcast ephemeris can be achieved at <ftp://ftp2.csno-tarc.cn/cnav/2022/> (accessed on from 28 January 2022 to 5 February 2022), and the PPP-B2b data were received by the K803 board from the SinoNav company ([www.sinognss.com](http://www.sinognss.com) (accessed on from 28 January 2022 to 5 February 2022)). The experimental data including the TJU-01 onboard GNSS data (accessed on from 28 January 2022 to 5 February 2022) presented in this study are available by contacting the corresponding author with reasonable request.

**Acknowledgments:** We are very grateful to the International GNSS Service (IGS) for providing the muti-GNSS data and products.. Thanks a lot to TianJin Yunyao Aerospace Technology Corporation for providing the TJU-01 onboard GNSS data.

**Conflicts of Interest:** The authors declare no conflicts of interest.

## References

1. Lee, B.-S.; Yoon, J.-C.; Hwang, Y.; Kim, J. Orbit determination system for the kompsat-2 using gps measurement data. *Acta Astronaut.* **2005**, *57*, 747–753. [[CrossRef](#)]
2. Montenbruck, O.; Ramos-Bosch, P. Precision real-time navigation of leo satellites using global positioning system measurements. *GPS Solut.* **2007**, *12*, 187–198. [[CrossRef](#)]
3. Yang, Y.; Yue, X.; Dempster, A.G. Gps-based onboard real-time orbit determination for leo satellites using consider kalman filter. *IEEE Trans. Aerosp. Electron. Syst.* **2016**, *52*, 769–777. [[CrossRef](#)]
4. Reichert, A.; Meehan, T.; Munson, T. Toward decimeter-level real-time orbit determination: A demonstration using the sac-c and champ spacecraft. In Proceedings of the 15th International Technical Meeting of the Satellite Division of The Institute of Navigation (ION GPS 2002), Los Angeles, CA, USA, 4–7 February 2002; pp. 1996–2003.
5. Montenbruck, O.; Hauschild, A.; Andres, Y.; von Engeln, A.; Marquardt, C. (near-) real-time orbit determination for gnss radio occultation processing. *GPS Solut.* **2013**, *17*, 199–209. [[CrossRef](#)]
6. Xiong, C.; Lu, C.; Zhu, J.; Ding, H. Orbit determination using real tracking data from fy3c-gnos. *Adv. Space Res.* **2017**, *60*, 543–556. [[CrossRef](#)]
7. Tang, J.; Lyu, D.; Zeng, F.; Ge, Y.; Zhang, R. Comprehensive analysis of ppp-b2b service and its impact on bds-3/gps real-time ppp time transfer. *Remote Sens.* **2022**, *14*, 5366. [[CrossRef](#)]
8. Liu, Y.; Yang, C.; Zhang, M. Comprehensive analyses of ppp-b2b performance in china and surrounding areas. *Remote Sens.* **2022**, *14*, 643. [[CrossRef](#)]
9. Ren, Z.; Gong, H.; Peng, J.; Tang, C.; Huang, X.; Sun, G. Performance assessment of real-time precise point positioning using bds ppp-b2b service signal. *Adv. Space Res.* **2021**, *68*, 3242–3254. [[CrossRef](#)]
10. Tang, C.; Hu, X.; Chen, J.; Liu, L.; Zhou, S.; Guo, R.; Li, X.; He, F.; Liu, J.; Yang, J. Orbit determination, clock estimation and performance evaluation of bds-3 ppp-b2b service. *J. Geod.* **2022**, *96*, 60. [[CrossRef](#)]
11. Tao, J.; Liu, J.; Hu, Z.; Zhao, Q.; Chen, G.; Ju, B. Initial assessment of the bds-3 ppp-b2b rts compared with the cnes rts. *GPS Solut.* **2021**, *25*, 131. [[CrossRef](#)]
12. Xu, Y.; Yang, Y.; Li, J. Performance evaluation of bds-3 ppp-b2b precise point positioning service. *GPS Solut.* **2021**, *25*, 142. [[CrossRef](#)]
13. Yang, Y.; Ding, Q.; Gao, W.; Li, J.; Xu, Y.; Sun, B. Principle and performance of bdsbas and ppp-b2b of bds-3. *Satell. Navig.* **2022**, *3*, 5. [[CrossRef](#)]
14. Yang, Y.; Liu, L.; Li, J.; Yang, Y.; Zhang, T.; Mao, Y.; Sun, B.; Ren, X. Featured services and performance of bds-3. *Sci. Bull.* **2021**, *66*, 2135–2143. [[CrossRef](#)]

15. Chen, J.; Zhang, Y.; Yu, C.; Wang, A.; Song, Z.; Zhou, J. Models and performance of sbas and ppp of bds. *Satell. Navig.* **2022**, *3*, 4. [[CrossRef](#)]
16. Wermuth, M.; Hauschild, A.; Montenbruck, O.; Kahle, R. Terrasar-x precise orbit determination with real-time gps ephemerides. *Adv. Space Res.* **2012**, *50*, 549–559. [[CrossRef](#)]
17. Xiao, G.; Liu, G.; Ou, J.; Zhou, C.; He, Z.; Chen, R.; Guo, A.; Yang, Z. Real-time carrier observation quality control algorithm for precision orbit determination of leo satellites. *GPS Solut.* **2022**, *26*, 102. [[CrossRef](#)]
18. Li, D.; Zhou, X.; Li, K. Centimeter-level orbit determination of grace-c using igs-rts data. *Remote Sens.* **2023**, *15*, 1832. [[CrossRef](#)]
19. Yang, H.; He, X.; Ferreira, V.; Ji, S.; Xu, Y.; Song, S. Assessment of precipitable water vapor retrieved from precise point positioning with ppp-b2b service. *Earth Sci. Inform.* **2023**, *16*, 315–328. [[CrossRef](#)]
20. Li, M.; Xu, T.; Shi, Y.; Wei, K.; Fei, X.; Wang, D. Adaptive kalman filter for real-time precise orbit determination of low earth orbit satellites based on pseudorange and epoch-differenced carrier-phase measurements. *Remote Sens.* **2022**, *14*, 2273. [[CrossRef](#)]
21. Li, B.; Ge, H.; Ge, M.; Nie, L.; Shen, Y.; Schuh, H. Leo enhanced global navigation satellite system (legnss) for real-time precise positioning services. *Adv. Space Res.* **2019**, *63*, 73–93. [[CrossRef](#)]
22. Förste, C.; Bruinsma, S.; Flechtner, F.; Abrykosov, O.; Dahle, C.; Marty, J.; Lemoine, J.; Biancale, R.; Barthelmes, F.; Neumayer, K. Eigen-6c3—the latest combined global gravity field model including goce data up to degree and order 1949 of gfz potsdam and grgs toulouse. In Proceedings of the AGU Fall Meeting Abstracts, San Francisco, CA, USA, 5–9 December 2011; p. G51A-0860.
23. Luzum, B.; Petit, G. The iers conventions (2010): Reference systems and new models. In Proceedings of the IAU General Assembly, Beijing, China, 20–31 August 2012.
24. Spiridonov, E.; Vinogradova, O.Y. Oceanic tide model fes2014b: Comparison with gravity measurements. *Izv. Atmos. Ocean. Phys.* **2020**, *56*, 1432–1446. [[CrossRef](#)]
25. Altamimi, Z.; Rebischung, P.; Collilieux, X.; Métivier, L.; Chanard, K. Itrf2020: An augmented reference frame refining the modeling of nonlinear station motions. *J. Geod.* **2023**, *97*, 47. [[CrossRef](#)]
26. Yang, Y.; Li, J.; Wang, A.; Xu, J.; He, H.; Guo, H.; Shen, J.; Dai, X. Preliminary assessment of the navigation and positioning performance of beidou regional navigation satellite system. *Sci. China Earth Sci* **2014**, *57*, 144–152. [[CrossRef](#)]
27. Montenbruck, O.; Steigenberger, P.; Hauschild, A. Multi-gnss signal-in-space range error assessment—methodology and results. *Adv. Space Res.* **2018**, *61*, 3020–3038. [[CrossRef](#)]
28. Xu, X.; Nie, Z.; Wang, Z.; Zhang, Y.; Dong, L. An improved bds-3 ppp-b2b positioning approach by estimating signal in space range errors. *GPS Solut.* **2023**, *27*, 110. [[CrossRef](#)]

**Disclaimer/Publisher’s Note:** The statements, opinions and data contained in all publications are solely those of the individual author(s) and contributor(s) and not of MDPI and/or the editor(s). MDPI and/or the editor(s) disclaim responsibility for any injury to people or property resulting from any ideas, methods, instructions or products referred to in the content.

Copyright of Remote Sensing is the property of MDPI and its content may not be copied or emailed to multiple sites or posted to a listserv without the copyright holder's express written permission. However, users may print, download, or email articles for individual use.